PERSPECTIVE

Check for updates

Unravelling complex mechanisms in materials processes with cryogenic electron microscopy

Minyoung Lee, [ab] Yonggoon Jeon, [ID][abc] Sungin Kim, [abd] Ihnkyung Jung, [ab] Sungsu Kang, [abe] Seol-Ha Jeong*[a] and Jungwon Park [ID] *[abfg]

Investigating nanoscale structural variations, including heterogeneities, defects, and interfacial characteristics, is crucial for gaining insight into material properties and functionalities. Cryogenic electron microscopy (cryo-EM) is developing as a powerful tool in materials science particularly for non-invasively understanding nanoscale structures of materials. These advancements bring us closer to the ultimate goal of correlating nanoscale structures to bulk functional outcomes. However, while understanding mechanisms from structural information requires analysis that closely mimics operation conditions, current challenges in cryo-EM imaging and sample preparation hinder the extraction of detailed mechanistic insights. In this Perspective, we discuss the innovative strategies and the potential for using cryo-EM for revealing mechanisms in materials science, with examples from high-resolution imaging, correlative elemental analysis, and three-dimensional and time-resolved analysis. Furthermore, we propose improvements in cryo-sample preparation, optimized instrumentation setup for imaging, and data interpretation techniques to enable the wider use of cryo-EM and achieve deeper context into materials to bridge structural observations with mechanistic understanding.

Introduction

Materials at the nanoscale often exhibit unique properties driven by surface[1–5] or quantum effects[6–8] that influence the macroscopic properties of chemistry-based processes, such as those in energy storage systems,[9,10] catalysis,[11–15] biochemistry,[16] self-assembly[17] or crystallization.[18–22] In solid materials, heterogeneities in morphology, presence of defects,[10,23] and interfacial characteristics[24–26] contribute to bulk properties in complex ways. Examples include nanoscale crystallinity affecting diffusive properties[27,28] or molecular structural variations giving rise to macroscale morphologies.[20,29,30] Gaining insight into how these unique nanoscale structures affect macroscopic characteristics allows for designing materials with

tailored functionalities, enhancing materials performance across various fields.

Investigation of such nanoscale structural variations requires characterization techniques capable of sub-nanometer resolution. Among such tools is cryogenic electron microscopy (cryo-EM), recognized by the Nobel Prize in Chemistry for its application in determining structures of proteins and biological organelles in their vitrified native states.[31] The technique involves rapidly freezing samples near liquid nitrogen temperature, which fixes the samples of interest within a thin layer of vitreous ice. This allows for the 3D structure analysis of proteins based on numerous solvated particle projections acquired by transmission electron microscopy (TEM) maintained at cryogenic temperatures. Cryo-EM have been widely utilized for elucidating mechanisms of biomolecular interactions through single particle analysis with 2D projections,[31] and even with *in situ* visualization of cellular processes enabled by cryo-electron tomography.[20] Despite the sensitivity of biomaterials to environmental conditions and the electron beam in electron microscopy, cryo-EM had enabled their imaging at unprecedented resolution. With the extensive use of cryo-EM for structural biology, the automation of sample preparation,[32–34] advancements in instrumentation,[35,36] and algorithms for image processing[37–40] have led to improvements in image quality, and as a result, deepened the level of structural investigation. These methods are currently well-established into a pipeline for efficient data acquisition.

[a]Department of Chemical and Biological Engineering, and Institute of Chemical Processes, Seoul National University, Seoul 08826, Republic of Korea. E-mail: jungwonpark@snu.ac.kr; jsh528@snu.ac.kr

[b]Center for Nanoparticle Research, Institute for Basic Science (IBS), Seoul, 08826, Republic of Korea

[c]Department of Physics and Chemistry, Korea Military Academy (KMA), Seoul 01805, Republic of Korea

[d]Department of Chemistry and Chemical Biology, Cornell University, Ithaca, NY 14853, USA

[e]Department of Chemistry, University of Chicago, Chicago, IL 60637, USA

[f]Institute of Engineering Research, Seoul National University, Seoul, 08826, Republic of Korea

[g]Advanced Institute of Convergence Technology, Seoul National University, Suwon, 16229, Republic of Korea

In materials science, imaging vitrified samples using cryo-EM had been initially utilized for the observation of the structures of solvated soft matter such as block copolymers,[41–43] surfactant micelles,[44] and single-walled carbon nanotubes.[45] These previous observations of assembled structures using cryo-EM span scales of hundreds of nanometers down to sub-nanometer scales,[46] allowing spatial resolutions sufficient for revealing individual assembly components at the nanoscale.[46] While cryo-EM initially focused on structures of soft matter, cryo-EM later expanded to observing a wider range of materials
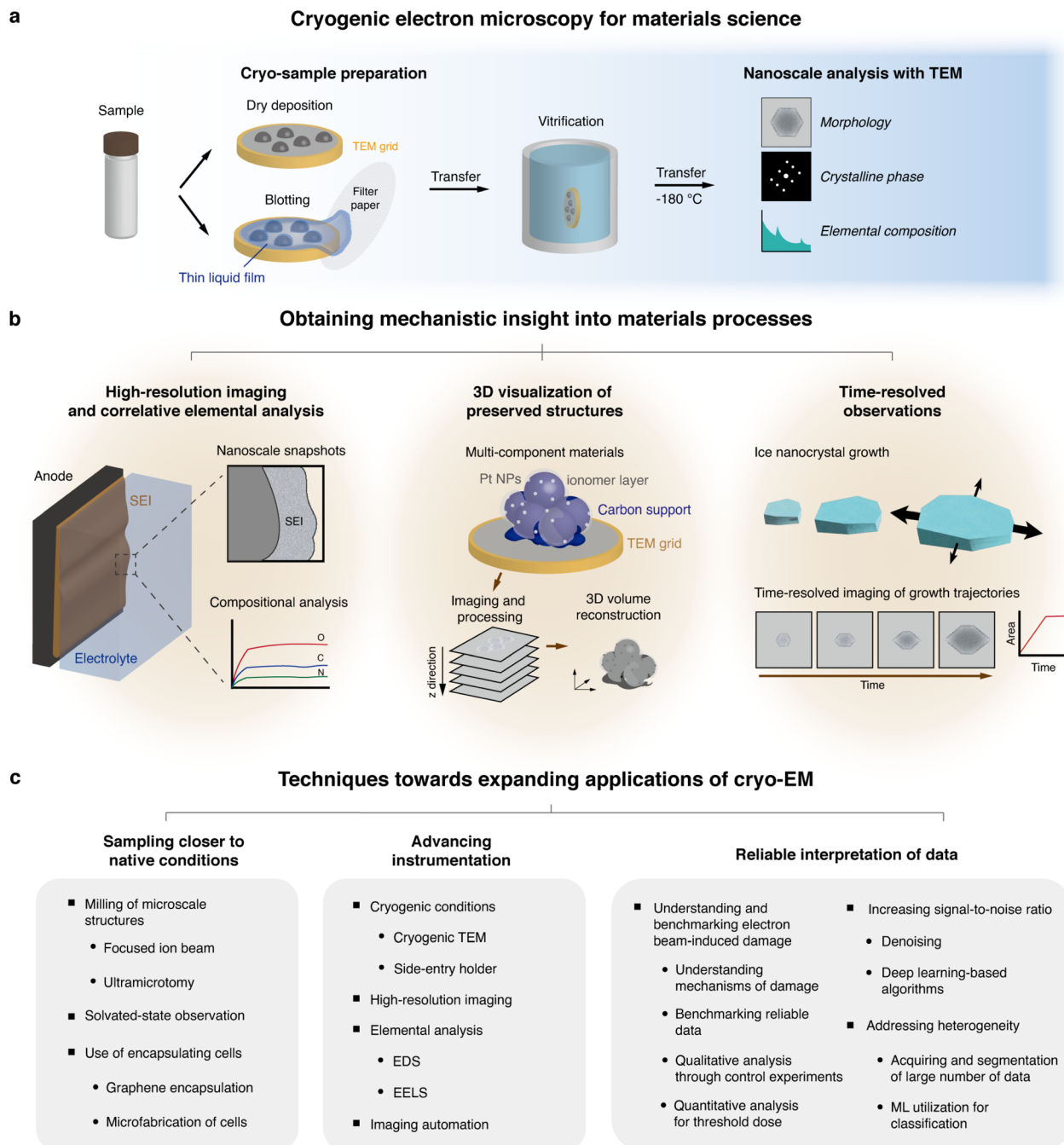

Fig. 1 An overview of the use of cryo-EM for applications in materials science, and the necessary improvements for cryo-EM use as a standard technique for materials analysis. (a) Scheme for cryo-EM use in materials science. The first step is sample preparation, which involves depositing the sample onto a TEM grid, where the excess liquid can either be completely dried, or can be blotted away with a filter paper, leaving a thin liquid film that can be vitrified with the samples. The samples are then cooled using a cryogen. The cooled samples are then transferred to a TEM, where the morphologies, phases, and elemental compositions can be analyzed. (b) Obtaining mechanistic insights from cryo-EM with (1) high-resolution imaging and correlative elemental analysis such as battery processes, (2) 3D visualization of complex structures such as a PEMFC fuel cell catalyst, and (3) time-resolved observations such as ice nanocrystal growth. (c) A list of the necessary improvements for using cryo-EM as a standardized analytical tool for conventional materials science analysis.

including inorganic materials and composites,[20,46,47] naturally expanding into the mechanistic studies of these materials in context of their operation in applications. Imaging using the TEM or scanning TEM (STEM) mode inherently provides structural information, and while structures of materials are closely tied to their functionalities and mechanisms in processes, bridging the gap between structural information and mechanisms of action is a prevalent goal. Therefore, there has been a growing need for obtaining more context beyond nanoscale structural information, such as higher resolutions down to atomic scale or multi-dimensional information such as correlative spectroscopic analysis or time-resolved information. The process of interpreting data is also crucial for deriving mechanistic understanding from structural data.

High-resolution analysis of inorganic materials has been performed with dry-state, conventional aberration-corrected TEM or STEM, which can be combined with energy-dispersive X-ray spectroscopy (EDS) and electron energy loss spectroscopy (EELS) to simultaneously retrieve elemental and chemical bonding information. Hence, various mechanisms in materials processes have been unveiled by investigating structures of functional materials at various length scales.[9,48,49] However, a large portion of materials processes operate in interface with solutions,[50,51] which may be altered by the ultrahigh vacuum conditions in electron microscopes when investigated using EM.[52] In materials that exhibit weaker chemical bonds, the effects from the electron beam can deteriorate sample integrity.[53,54] The key difference between cryo-EM and conventional EM is that cryo-EM techniques involve freezing samples and preserving their native states,[18] while minimizing electron beam-induced reactions.[26,47,55] This enables more accurate data acquisition regarding material structures in their operational conditions. Samples for cryo-EM analysis are normally deposited or transferred to a grid, which are then cooled by plunging into a cryogen at liquid nitrogen temperature and transferred to a side-entry cryo-transfer holder (Fig. 1a).[26,56]

As such, cryo-EM had broadened our understanding of material structures in near-native conditions. Currently, the field is moving towards gaining fundamental understanding of nanoscale structures and linking these insights to material mechanisms that are important in real-world applications[47] (Fig. 1b). However, this task is complicated by the extensive sample preparation requirements for cryo-EM, such as thinning, which may inadvertently alter the native state of the samples. Additionally, deeper understanding on the interaction between the electron beam and low-temperature, solution phase samples, the accurate interpretation of the data,[47] as well as a current lack of widespread instrumental capabilities that enable high-resolution imaging or elemental analysis are key limitations that must be improved[57] (Fig. 1c).

In this Perspective, we highlight the advantages of cryo-EM for its potential in elucidating operational mechanisms of specific material systems at the nanoscale by utilizing high-resolution imaging, correlative elemental analysis, three-dimensional and time-resolved analysis to further bridge the gap between structural observations and mechanistic understanding. We additionally discuss innovations needed in cryo-

sample preparation, data interpretation, and instrumentation. These enhancements aim to allow for standardized use of cryo-EM in materials science, improving the applicability of cryo-EM for unveiling unknown mechanisms in materials science.

Obtaining mechanistic insight into materials using cryo-EM imaging methods

Utilizing cryo-EM has enabled imaging intricate nanoscale structures of a variety of materials by mitigating two issues associated with TEM imaging – (1) reducing structural changes due to the imaging electron beam and (2) maintaining the sample in solution state under the high vacuum of the TEM. The first challenge is associated with the inevitable knock-on, radiolysis or thermal damage from the electron beam.[58] Through multiple studies on different materials, especially organic materials[59,60] or Li dendrites,[26] it was found that cooling the specimen near liquid nitrogen temperature reduces structural damage during imaging. The second challenge of conventional TEM is from the vacuum environment, which limits imaging to dry samples. The advantages of cryo-EM, which involves obtaining "snapshots" of solution-based processes in frozen-state, allows for us to obtain structural insights with the use of higher electron doses for high-resolution imaging, as well as longer electron exposure times for elemental mapping of beam-sensitive or metastable regions of the sample.[61,62] Cryo-EM has been applied to observing the sub-nanometer-scale structures of various beam-sensitive materials, including metal organic frameworks (MOFs),[54,63,64] zeolites,[65] or perovskites,[66–68] which have exhibited significantly less structural change arising from electron beam-induced damage compared to using conventional TEM. These results provide opportunities for the structures of fragile materials to be characterized with TEM.

Beyond the structural information provided by projection images, there has been a growing need for obtaining more comprehensive data to derive meaningful mechanistic insights. Higher resolutions down to atomic scale, multi-dimensional information such as correlative spectroscopic analysis or time-resolved information offer promising methods for obtaining more context into materials. However, these methods are also currently associated with challenges in sample preparation, data interpretation, and instrumentation. In this section, we discuss the recent advancements and the opportunities for overcoming these challenges, with the overarching goal of enhancing mechanistic understanding in materials sciences through cryo-EM.

Cryogenic high-resolution TEM (HRTEM) and correlative elemental analysis

A crucial aspect to consider in analyzing materials processes is understanding not only the structure, but also the atomic components and their spatial arrangements in a material. In this aspect, HRTEM enables the visualization of materials at atomic scales, including phases or defects that contribute to the

bulk properties of a material. The incorporation of cryogenic temperatures to these high-resolution techniques is critical because the method utilizes high electron doses that damage many fragile samples. The damage mitigation effects of cryo-EM also bring opportunities for the use of energy dispersive X-ray spectroscopy (EDS) and electron energy loss spectroscopy (EELS) for elemental analysis. EDS is used to obtain information on the elemental composition of the samples, while a region of the sample can be selected to produce a map of elements present. However, EDS normally require relatively higher electron doses and repeated exposures to collect signal from sample, and these limitations could benefit from the use of cryo-EM. For systems that exhibit inelastic scattering of electrons at low energies, EELS elemental analysis can be performed for materials that exhibit energy loss at low energy loss regions, and can be a viable option that is more dose-efficient.[69] Additionally, EELS vibrational spectroscopy is sensitive to the chemical states or the phases for certain materials,[70] enabling their observation correlatively with the structure images obtained with TEM. We specifically highlight the opportunities for mechanistic understanding with cryo-EM by using cases from two fields – battery chemistry and quantum materials, as examples for high-resolution observations and correlative spectroscopic analysis.

Analysis for battery mechanisms

A prominent field that utilizes high resolution and elemental analysis with cryo-EM is for elucidating operation mechanisms in batteries. Batteries, which work through transport of ions and electrons in an assembly of the anode, cathode, electrolyte, and separator, contain highly-reactive components that give rise to unique interfaces in the regions of contact between those compartments.[71,72] Particularly, Li plating at the anode is affected by the presence of the solid electrolyte interphase (SEI), a nanoscale passivation layer formed from the reaction between surface Li and electrolytes. The SEI governs the transport of Li from the electrolyte to the Li metal surface,[73–75] and also affects the resultant structures of Li dendrites, which are main causes of battery failure and safety concerns.[72] Despite this significance, observation of SEI has been limited using conventional TEM because Li metals and the SEI are severely fragile toward the electron beam. The issue becomes worse as higher electron dose rates are used for high magnification imaging. In pioneering work by Li et al., the incorporation of cryogenic temperatures has enabled Li dendrites to be observed with high-resolution TEM, revealing the lattice structure of Li and the presence of defects in areas with kinks (Fig. 2a).[26] In addition, as the Li dendrites can be deposited directly from a coin cell,[78,79] the structures of the SEI that has arisen from the operating conditions could be obtained. SEI interfaces, which are generally amorphous with nanoscale inorganic domains such as Li_2O or Li carbonates, can be characterized with imaging (Fig. 2b) and EELS (Fig. 2c).[78,80,81] With these methods, insights into the structures and compositions of the SEI could be obtained (Fig. 2d), which also influence the shapes of Li dendrites.[73,76,82] SEI properties have been found to change with

different types of electrolytes used (namely ether-based[81,83] and carbonate-based[81,84] electrolytes), at the presence of electrolyte additives,[76,85] or different current densities.[73,86] Specifically, the distribution of organic and inorganic domains, thickness, and layered structures of the SEI can affect its mechanical properties and the diffusion dynamics of Li within the SEI, influencing the Li plating process during deposition. This insight is relevant to enhancing the performance of Li metal batteries by improving function through SEI engineering.[87–89] In one example, Gao et al. demonstrates such SEI engineering that resulted in a high-performance Li metal battery under low temperature at high rate-charging conditions (Fig. 2e).[77] Cryo-EM images of the SEI reveal a multilayer SEI that effectively seals the Li surface at low temperatures, improving its performance (Fig. 2f).[77]

As such, cryo-EM provides opportunities for evaluation of SEI structures in various cycling conditions. Beyond Li deposition in battery chemistry, cryo-EM may also be used to study calendar aging,[90] a significant failure mode where an active material left in contact with the electrolyte degrades over time. Another less-understood structure to visualize with the cryo-EM is the cathode electrolyte interface, which has been shown to contribute to stable cycling in a Li-sulfurized polyacrylonitrile cathode.[91]

Elucidating atomic origins of properties in quantum materials

High-resolution observations are crucial for understanding the atomic-scale mechanisms behind the unique properties of quantum materials. These properties, which include superconductivity, topological states or colossal magnetoresistivity,[92] are primarily governed by the electronic, magnetic, or lattice order within the materials.[93] At the nanoscale, many of these states coexist, yet the complex interplay between them remains elusive. Observing these materials at cryogenic temperatures is crucial as it preserves the phases and properties that only manifest at low temperatures, and suppresses thermal vibrations of atoms. Liquid N_2 and liquid He holders, developed decades ago, enable these low temperature observations within electron microscopes.[92] In one of the earlier works, tetragonal and orthorhombic phases of a $La_{2-x}Ba_xCuO_4$ cuprate were investigated at temperatures as low as 20 K with a liquid He holder, using electron diffraction and dark-field imaging to reveal the formation of twin boundaries at low temperatures.[94]

The demand for higher resolutions in cryo-EM for quantum materials is driven by the need to observe fine structural features down to the picometer-scale displacements of individual atoms that give rise to the unique properties.[95] Recent advances in aberration-corrected cryo-STEM have enabled significant improvements in spatial and spectral resolution. A major challenge behind high resolution imaging is specimen drift caused by the cooling holder or the sample stage, which must be addressed as it leads to a loss in resolution. One approach demonstrated by Savitzky et al. proposed imaging with fast frame rates and employing a post-imaging drift correction algorithm, which performs cross-correlation analysis of low signal images for accurate frame alignment.[96] The
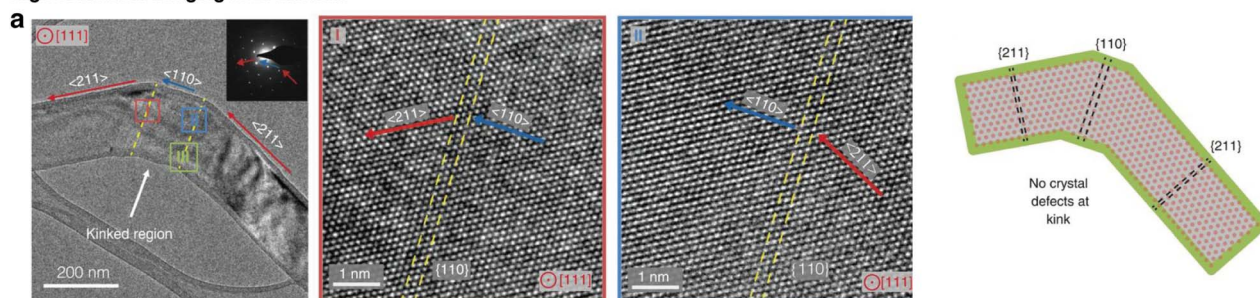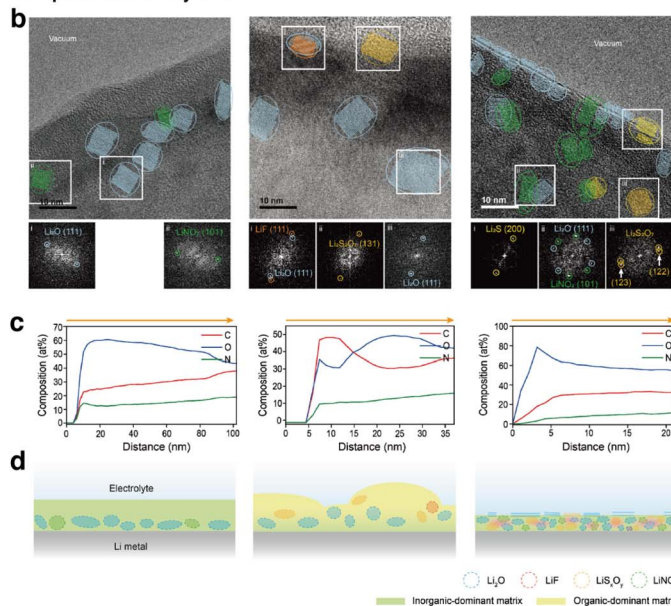
Fig. 2 High-resolution cryo-EM and correlative elemental analysis of battery materials for understanding operation mechanisms. (a) High-resolution imaging of a Li dendrite at the region of a kink, revealing local crystallographic properties of the Li dendrite (reproduced with permission from ref. 26, copyright 2017 AAAS). (b) Images of the SEI revealing areas with local crystallinity, in which the crystallographic phases are determined using fast Fourier transform patterns. (c) Composition profile of C, O, N along the depth of the SEI. (d) Predicted morphologies and composition of the SEI based on cryo-EM analysis (reproduced from ref. 76, copyright 2024 ACS Publications). (e) Scheme for an example of SEI engineering for improving battery performance. (f) Characterization of the SEI for revealing the role of SEI on performance (reproduced from ref. 77, copyright 2020 Nature Publishing Group).

picometer-scale resolution achieved with this method has particularly beneficial for observing one class of quantum material phases, known as charge-ordered phases, in which electrons and the atomic lattice form periodic patterns that break the translational symmetries of the crystal.[93] These phenomena are closely linked to the material's properties that may influence superconductivity or other electronic behaviors such as colossal magnetoresistance and metal–insulator transitions.

The states of a transition metal dichalcogenide 1T′-TaTe$_2$ (Fig. 3a–c) was imaged with high-resolution cryo-STEM to reveal the presence of Ta trimer states at 93 K, which are not present at room temperature (Fig. 3d and e). Fourier transforms were used to compare images obtained in the two temperature regimes and reveal the presence of a modulated structure in the lattice at low temperatures (Fig. 3c and d).[97] In a different example,

periodic lattice displacements of a charge-ordered manganite, $Nd_{1/2}Sr_{1/2}Mn_2O_3$ was mapped to reveal the existence of an intermediate state of electrons that contain both site and bond order and breaks inversion symmetry. The images of atoms in their intra-unit-cell arrangements enable the understanding of charge ordering through displacement pattern analysis with group theory.[98]

While structures at very high resolutions were observed for different temperatures of quantum materials so far, the quest for leveraging cryo-EM in elucidating mechanisms for a variety of quantum material systems necessitates increasing the versatility of the imaging technique. For instance, finer control of temperature of the sample would be essential for investigating the dynamics of electronic phases at multiple different temperatures.[47,93,99] Moreover, correlative spectroscopic analysis such as EELS at atomic scales could provide additional insight
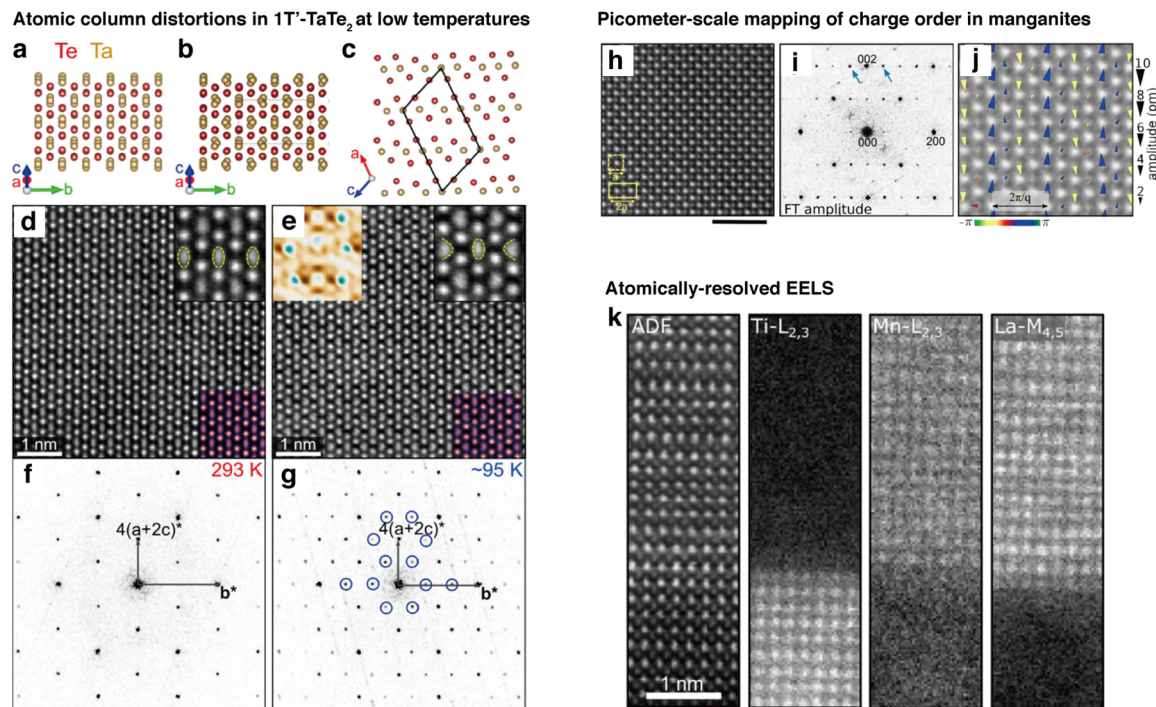
Fig. 3 High-resolution, low temperature imaging of atomic columns of quantum materials. (a–c) Models of the structure of 1T'-TaTe$_2$ at (a) room temperature and (b) low temperatures. (c) Lattice model indicating the monoclinic unit cell. (d and e) STEM image at (d) 293 K and (e) 95 K. The insets at the top right are magnified views of images, and the insets at the bottom right are multislice simulations of HAADF-STEM images. The inset at the top left of (e) is the intensity difference map. (f and g) Fourier transforms of the STEM images at (f) 293 K and (g) 95 K. Blue circles represent superlattice peaks. (h–j) Picometer-scale mapping of charge order of Nd$_{1/2}$Sr$_{1/2}$Mn$_2$O$_3$ with (h) HAADF-STEM image at 95 K, (i) corresponding fast Fourier transform image, and (j) map of the periodic lattice displacements. (k) Atomically-resolved EELS of La$_{0.8}$Sr$_{0.2}$MnO$_3$/SrTiO$_3$ (reproduced with permission from ref. 93, copyright 2021 ACS Publications).

into electronic structures beyond the images from STEM (Fig. 3k).[93,100] However, a major challenge is the additional drift[101] that would be introduced with these two techniques due to the heating process of side-entry holders for variable temperature experiments, and the longer frame dwell times required for EELS.[102] While direct electron detectors have mitigated some of these effects with faster readout times, further advancements in drift correction will be crucial for high-resolution imaging of a wide variety of quantum materials.

The capabilities offered by cryogenic conditions in high-resolution imaging and correlative spectroscopic analysis are pivotal not only for battery chemistry and quantum materials, as discussed, but also for a broader range of systems in materials science. High-resolution cryo-EM is beneficial for imaging crystalline materials, as it reveals interfaces, defects, or structural modulations at atomic levels that dictate material properties. Correlative spectroscopic analysis further enhances this by localizing elements that are present for multicomponent systems, revealing how different components interact and influence material behavior during operation.

## Visualizing structural heterogeneities in three dimensions

Heterogeneity inherent in nanoscale structures of materials plays crucial roles in determining the mechanical[103] and mass transport[104] properties. Local enhancements or depletions of

specific properties combine to influence the overall behaviors and mechanisms. Thus, probing the 3D structures of various material components is essential for understanding bulk chemistries. For example, in the context of designing catalysts, key questions include how nanoparticles are dispersed on the substrate[105] and whether they are embedded within the pores,[106] because the performance of the catalyst rely on the spatial distribution of catalytically active nanoparticles within the support. However, retrieving information along the depth direction parallel to the electron beam path is challenging with two-dimensional projections of the TEM. To accurately understand these 3D properties, additional cryo-EM sample preparation techniques and selecting suitable imaging modalities for visualizing materials in three dimensions are important.

Ultramicrotomy sectioning. Micrometer-sized materials can be sectioned by ultramicrotomy, in which materials are embedded in a solid medium such as resin and sectioned with nanoscale thickness for observation within the cryo-EM (Fig. 4a).[65] In one example, Kim et. al. observed the dispersion of PdO clusters within the pores of SSZ-13 zeolites through sectioning the catalyst sample using ultramicrotomy and imaging the interior structures using cryogenic STEM (Fig. 4b).[65] Sectioning had enabled the visualization of PdO clusters that were embedded inside the zeolite pores, while the cryogenic conditions additionally mitigate beam damage of the beam-sensitive substrate. Through this technique, the
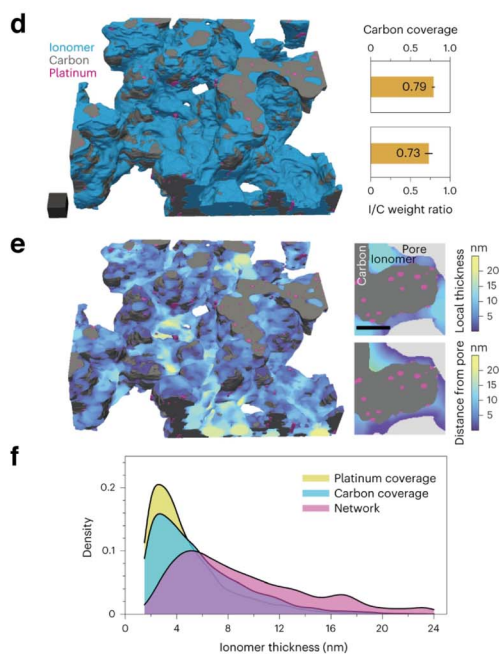
Ultramicrotomy sectioning
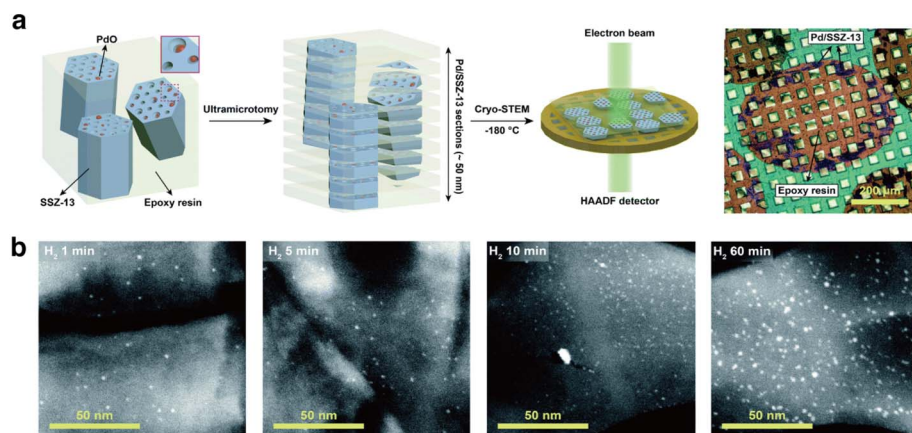
Cryo-ET
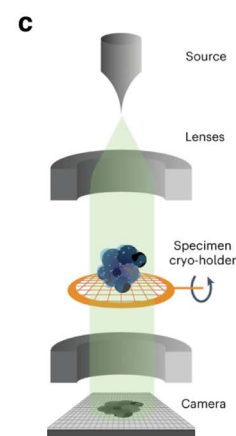
3D morphology of catalyst layers

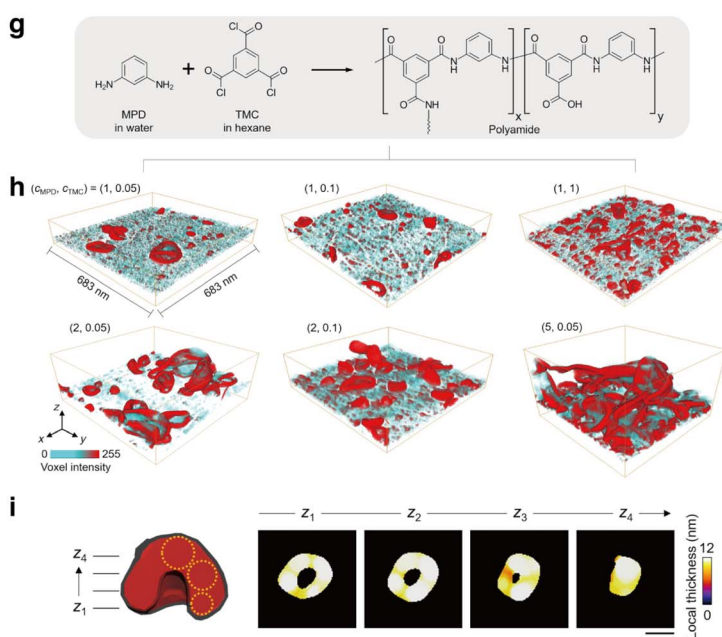**Morphological quantification for performance prediction**

Fig. 4 Techniques for associating 3D morphology with functional outcomes for preserved structures enabled by cryo-EM. (a) Schematic of the ultramicrotomy sectioning process of SSZ-13 to visualize PdO clusters embedded within the pores of the support. (b) Cryo-STEM images of sections according to different H_2 treatment times (reproduced with permission from ref. 65, copyright 2021 Royal Society of Chemistry). (c) Schematic of a cryo-ET experiment. (d) 3D map of a catalyst obtained using cryo-ET, and analysis of 3D distribution of ionomers enabled by cryo-ET. (e) Map of local thickness of ionomers on the catalyst. (f) Distribution of the ionomer thickness plotted for different sampling and calculation methods. (Reproduced with permission from ref. 107, copyright 2023 Nature Publishing Group). (g) Schematic for production of the polyamide membranes. (h) 3D maps of polyamide membranes with different monomer concentrations obtained with cryo-ET. (i) Schematic for quantification of 3D morphologies of crumples (reproduced with permission from ref. 108, copyright 2022 AAAS).

uniformity of the PdO clusters that were embedded within the pores of the zeolite could be quantified with minimal electron beam-induced damage. Furthermore, the morphological uniformity of the PdO clusters were associated with passive NO_x adsorbers and CH_4 combustion performances, where high monodispersity contributes to increased performance.[65]

Cryo-electron tomography (cryo-ET). 3D structures may also be obtained using cryo-electron tomography (cryo-ET), which involves acquisition of tilt-series images by utilizing stage tilt,

and then reconstructing 3D volumes from the image sequences (Fig. 4c).[107] While cryo-ET requires multiple exposures of a sample to the electron beam, low temperature conditions can mitigate the damage imposed on the samples. Girod *et. al.* demonstrated the use of cryo-ET along with deep-learning based segmentation to obtain the 3D structure of a proton-exchange membrane fuel cell (PEMFC) catalyst containing the carbon support, the Pt catalysts, and the ionomer layers (Fig. 4d). While catalyst systems are known to contain particles,

ionomer electrolytes, and void spaces between the catalyst and ionomer agglomerates, the 3D distribution of these components have remained elusive. Furthermore, ionomers are difficult to image using standard TEM techniques because of their beam-sensitivity. Through the 3D map obtained from cryo-ET, local thicknesses and distribution of ionomers on the catalyst have been determined (Fig. 4e and f). Such local structures are known to influence how protons or oxygen are transported within the ionomer layers into the Pt catalysts in contact with an electrolyte.[107,109,110] While ionomers have been observed with imaging and elemental analysis in the past,[111,112] this work further demonstrates the capability of imaging using cryo-TEM for 3D mapping and quantification of areas with minimal invasiveness. Utilizing the insights from this analysis, the carbon–ionomer interface could be engineered to unravel the relationships between the ionomer's conditions in dispersions and catalyst slurries, and the resultant morphology of the film and network within the catalyst layers.

3D volumes obtained from TEM could also be used to predict performance outcomes based on shape factors. In the work by An *et. al.*, polyamide membranes used for commercial molecular separation were imaged with cryo-ET to observe membrane crumpling morphologies with varying monomer concentrations (Fig. 4g and h).[108] Furthermore, membrane microenvironments were quantitatively measured with nanoscale morphological parameters to predict methanol permeability within the membranes (Fig. 4i).[108] In subsequent work by Kalutantirige *et. al.*, it was discovered that regions where two or more crumples meet exhibited thicker membrane walls, suggesting that crumples form through a coalescence mechanism where crumple walls connect and merge.[113] These observations were correlated with coarse-grained molecular dynamics (MD) simulations to verify the proposed membrane formation mechanisms. Furthermore, by using graph theory as a basis for quantifying interconnected crumples, the study proposes that structural rigidity trends monotonically with the mechanical robustness of the membranes, providing insights into the nano-structural architecture that influences performance at the bulk level.[113]

Determining the 3D morphology of materials provides another dimension for quantitative analysis for obtaining insights into structures that affect macroscopic properties. Techniques that acquire information in the depth direction can be adapted for imaging the interior of microscale particles, particularly those with complex internal architectures such as pores, or those composed of multiple components. Furthermore, 3D imaging can enhance the analysis of amorphous or anisotropically shaped materials by revealing the three-dimensional shapes that affect their bulk properties. By conducting correlative analysis of material performance and strategically integrating quantification parameters for analyzing nanoscale morphologies, the gap between structural data and mechanistic insights can be bridged.

Time-resolved observations of materials processes

Along with the nanoscale high spatial resolution cryo-EM offers, obtaining data along the temporal dimension is also crucial for developing a mechanistic understanding of how material structures form and evolve over time. Tracking changes over time enables understanding of nucleation mechanisms, important structural intermediates, and how final products are ultimately shaped. Time-resolved studies also provide insight into the kinetics and stability of phases at the nanometer scale, achieving deeper understanding of the dynamic processes that ultimately govern the behavior and functionality of complex materials.

Self-assembly and crystallized materials in solution. An advantage of cryo-EM is in its ability to observe structures that have been embedded in solution phase, allowing for the visualization of metastable, intermediate structures. This capability is particularly beneficial for observing self-assembly processes of polymeric[60,114] or organic materials,[115] as intermediates in these processes play an important role in determining the final structures of complex self-assembled materials. Classical nucleation theory fails to explain some of the mechanisms behind assembly processes.[116] In such non-classical processes, probing the intermediate stages is beneficial to elucidate how individual monomeric and oligomeric components assemble to produce functional materials.[20]

The intermediate stages of a self-assembly process occurring in solution can be probed using cryo-EM by producing aliquots of samples at different stages of assembly. For producing cryogenic samples, a few microliters of solution are extracted from each aliquot and deposited onto a TEM grid. The grid is then blotted with filter paper to produce a thin layer of liquid, and plunge-frozen in liquid ethane to produce a layer of frozen solution containing the structures to be observed. Sequentially imaging different time frames of the assembly process reveals the nanoscale structures in various intermediate stages. Owing to the versatility of the technique, formation mechanisms of a variety of materials systems have been revealed to obtain insights into synthetic mechanisms. In one example, the oriented attachment mechanism during self-assembly was revealed by cryo-EM imaging of cyclosporin A, which shows the intermediate structures of small crystals undergoing attachment to form a large mesocrystal (Fig. 5a–e).[115] In another example by Tsarfati *et. al.*, perylene diimide crystallization was observed, where densified spheres formed initially as shown in Fig. 5f and g. These spheres undergo an intermediate phase exhibiting faceted intermediates in Fig. 5h and i, and evolve into crystalline fibrillar structures in Fig. 5j and k. The scheme of the crystallization process in Fig. 5l suggests a densification process followed by crystallization that occurs within the dense phases, ultimately forming ordered fibrillar structures.[117] Other examples that use time-resolved cryo-EM analysis include early-stage biomimetic mineralization,[118–121] formation of MOFs,[122] hierarchical structural evolution,[123–125] oriented attachment processes,[126] chiral self-assembly,[127] and amorphous-to-ordered-phase transitions[18] by enabling time-resolved imaging for processes at time scales of minutes, hours, or even days.

In many self-assembly systems, however, cryo-EM observation of these intermediate structures faces challenges associated with the coexistence of multiple mechanisms at the nanoscale, obscuring the dominant mechanistic picture.[128] A

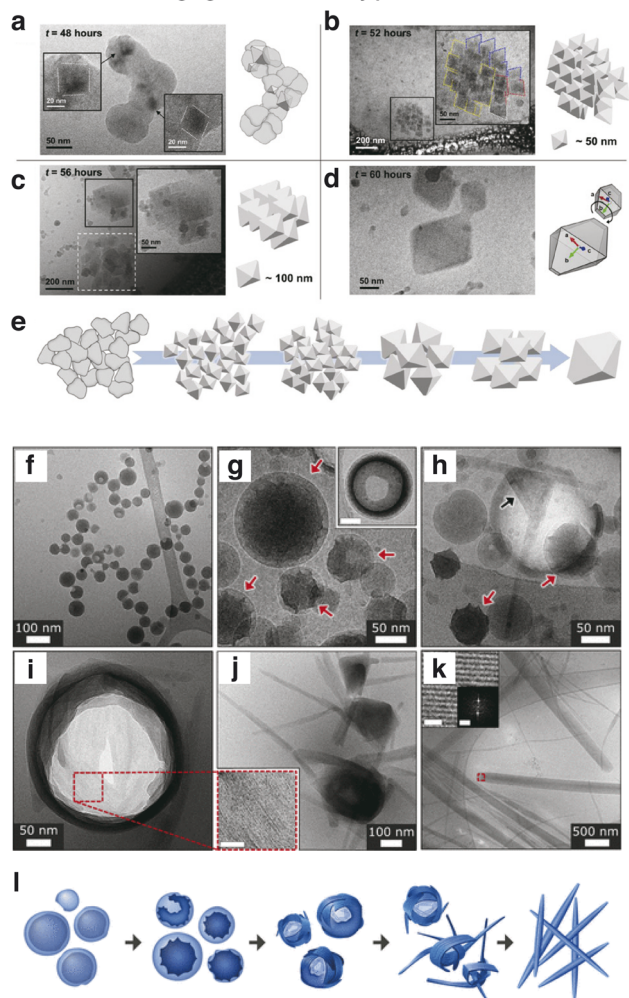**Time-resolved imaging of self-assembly processes**

Fig. 5 Time-resolved imaging of self-assembly processes. (a–d) Cryo-EM images of structures observed during self-assembly of cyclosporin A nanoparticles after (a) 48 h, (b) 52 h, (c) 56 h, and (d) 60 h after initiation (reproduced with permission from ref. 115, copyright 2022 ACS Publications). (e) Schematic of the proposed crystallization pathway. (f–k) Crystallization of perylene diimides (f) observed immediately, (g) observed after 30–50 min, (h) exhibiting faceted intermediate showing crystallinity, (i) with ruptured aggregate, (j) showing growth of fibrous crystals, and (k) fully developed. (l) Schematic of the proposed crystallization pathway (reproduced with permission from ref. 117, copyright 2018 ACS Publications).

wide range of heterogeneity of morphologies formed at the nanoscale complicates the interpretation of the assembly process. In addition, blotting of samples for thinning the solution can lead to damage of structures of embedded materials,[129] especially for larger, microscale assemblies. These limitations hinder the reliable observation of macroscale structures. To overcome these challenges, correlation of structures obtained from imaging with microscale analysis, such as with diffraction or scattering techniques are essential.[130] Particularly for larger structures, it is important to perform additional imaging analysis with larger-scale techniques, such as scanning electron microscopy (SEM)[131] or optical

microscopy[132] to ensure that samples are minimally affected by the sample preparation process. The blotting process of samples is difficult to avoid during conventional cryo-EM sampling procedures, but developments in sampling procedures that do not require blotting could improve the structural stability of these assemblies.

Direct observation of *in situ* processes at low temperatures. With cryo-EM, processes occurring at low temperatures can be directly imaged and characterized. One such example is the crystallization of ice. At low temperatures, a mix of ice crystal polymorphs, namely cubic and hexagonal ice, are present.[133] However, understanding the distinct behaviors of these nano-sized ice domains is challenging. Spatially-averaged techniques like X-ray diffraction renders deconvolution of the different crystalline phases difficult, while molecular-scale techniques such as molecular dynamics simulations are challenging to implement for nanoscale systems.[134]

Cryo-EM is therefore a valuable tool for bridging this resolution gap by allowing direct imaging at the nanoscale. Currently, ice nanocrystal growth has been visualized at cryogenic conditions by deposition of residual water vapor onto a graphene grid maintained at liquid nitrogen temperature, which induces a vapor-to-solid transition for observation. This approach has enabled molecular-scale visualization of ice growth processes on 2D materials substrate *in situ* (Fig. 6a and b).[135] In another study, amorphous ice was prepared by vitrifying a thin liquid film in liquid ethane, and ice crystallization was induced by heating amorphous ice to 143 K. This resulted in an amorphous-to-crystalline transition in a thin amorphous ice film (Fig. 6c). Snapshots of different regions of the ice film at different time periods were obtained, as shown in Fig. 6d, in order to mitigate electron beam damage. This study also tracks the growth of individual ice nanocrystals and correlates the results with MD simulations, revealing the growth anisotropy of heterocrystalline ice (Fig. 6e and f).[136] Specialized *in situ* cryo-EM techniques, such as the incorporation of laser-induced heating have also been used to observe various forms of H_2O, such as detecting the properties of deeply supercooled water before crystallization.[137,138]

Nano-to-molecular-scale observation of ice within the TEM is important in applications for ice growth optimization in various low-temperature systems such as cryopreservation materials. Whereas the energetics and the formation mechanisms of cubic and hexagonal ice remain poorly understood,[133,134,139,140] cryo-EM is emerging as a valuable tool for being able to track the structures and growth of ice crystals. This provides crucial insights into ice physics, where nanoscale ice crystals shape the formation of larger, microscale ice structures. Furthermore, studying the interaction between ice crystals and nanoscale materials using cryo-EM, particularly within biological macromolecules or cell membranes, is highly valuable. The formation of crystalline ice within cells that have been treated with different antifreezing agents have been achieved using cryo-EM, offering significant insights into antifreezing processes.[141–143]

Time-resolved analysis enables the direct monitoring of the structural changes over time to reveal process mechanisms or kinetics. Observing aliquots of samples undergoing operation
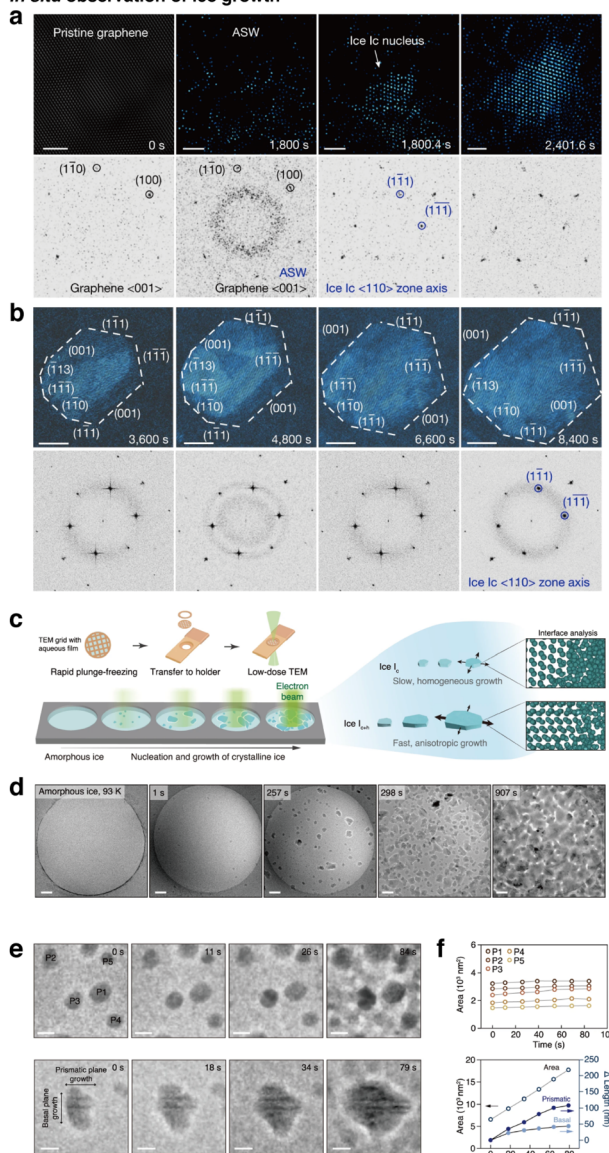
Fig. 6 Direct observation of *in situ* ice growth *via* individual particle tracking. (a and b) High-resolution TEM images and the corresponding FFTs for (a) nucleation of cubic ice from residual water vapor within the TEM column on a graphene surface and (b) a cubic ice nanocrystal with defined facets. (Reproduced with permission from ref. 135, copyright 2023 Nature Publishing Group). (c) Schematic for the observation of ice crystallization in amorphous ice films. (d) Snapshots of ice crystallization of a free-standing amorphous ice film at different annealing time periods at different locations. (e) Individual particle tracking of growth over time and (f) plots of particle growth over time (reproduced with permission from ref. 136, copyright 2023 Nature Publishing Group).

crystallization of ice, where the process temperature corresponds to temperatures compatible with cryo-EM. However, many materials processes do not undergo dynamics at these very low temperatures. One proposed technique for observing transient dynamics within the TEM is by melting the ice to allow configurations of molecules to change before the sample is revitrified again.[144] A technique for melting ice in the TEM using a laser beam has been demonstrated for viruses to observe their microsecond-scale structural dynamics.[145] Another method could involve freezing and thawing samples by increasing temperature, while maintaining the liquid and the sample encapsulated to prevent drying.[146] The development of new *in situ* techniques and directly tracking individual structural units over time will be beneficial for achieving mechanistic studies.

Technical developments for expanding applications of cryo-EM

Interpreting the effect of nanoscale structures on macroscopic properties have long been of interest for many materials science disciplines, which provide fundamental insight into how materials should be designed for tailored functionalities.[30] The implementation of cryo-EM has brought promising developments for the observation of materials with reduced structural changes that may have occurred from drying or electron beam effects. On another note, as demonstrated by An *et. al.*, nanoscale structural morphologies, even for highly amorphous shapes, can be quantified for correlation with their expected performances.[108] Cryo-EM has vast opportunities in materials science for obtaining images of nanoscale structures for this purpose, especially in their metastable states. However, cryo-EM use in materials science poses challenges due to the ultrathin sampling requirements, the small visualization area of the TEM, the static nature of cryogenic imaging, and beam-induced effects. Fortunately, advancements in instrumentation and pipelines for image processing for interpretation has been significantly developed for purposes in reconstructing 3D volumes of proteins for structural biology.[31] Such techniques can be modified and implemented to adapt to the benchmarking of cryo-EM analysis for materials science as well. However, there are other developments that are required specifically for materials science that we will also discuss in this section. These developments will allow the acquisition of image data under conditions that closely mirror the native environment, determining structure–function relationships for materials. Specifically, carefully designed model systems during sample preparation, as well as consideration in data interpretation and acquisition are necessary to realize data collection representative of realistic conditions using cryo-EM.

Sample preparation

Sectioning. A direct way to visualize the native-state mechanisms of operational processes with TEM is to extract samples directly from the working processes themselves. However, the challenge associated with sample preparation for such purposes is the requirement that samples must be ultrathin,

can be widely used because of its applicability to many different materials systems. However, these observations do not capture the evolution of individual structural units over time. Additionally, the heterogeneity within a sample, such as particles being at different stages of evolution within the same aliquot, complicates data interpretation. Tracking of *in situ* processes of individual units has been demonstrated, for instance, with the

preferably thinner than tens to hundreds of nanometers.[147] Many processes in materials science occur at much larger scales, rendering the observation of the process in its pure state difficult. As demonstrated in the earlier section with the example of depth-direction imaging of SSZ-13 zeolite particles using ultramicrotomy, fine milling techniques are valuable tools for producing thin samples and analyzing the spatial distribution of particles in the depth direction. Instead of milling a dry, resin-embedded sample, advancements in preparing frozen samples and performing milling under cryogenic conditions—techniques originally developed for biological studies—have become important improvements that can also be applied to materials science. Cryo-focused ion beam (FIB)[148] or cryo-ultramicrotomy[149] are two such methods that can be employed. These techniques have been used for observing 'snapshots' of cellular processes including viral entry into the cell membrane,[150] or distribution of proteins within the cell during a cellular response.[151] With molecules in context with the operational environment of the cell, mechanistic insights and the interplay between different components of the cellular system can be identified. However, there are still challenges in implementing these sectioning tools to materials systems. Firstly, limited understanding on the impact of freezing these bulk materials or solvents hinder the reliability of the sample preparation process at cryogenic temperatures.[152] If the material is especially prone to reacting with environmental oxygen or water vapor, the reliability of the data will be compromised.[56] Additionally, an important consideration for using FIB is associated with deposition of Ga from the Ga ion beam source used for milling, which may produce side reactions onto the surfaces of the samples and be manifested as artifacts during phase or elemental analysis.[56,153] Finally, these sectioning techniques are time-consuming and semi-manual, where producing a single section of a sample may take hours. In many purposes for cryo-EM observation, sectioning tools may be unnecessarily inefficient.

Preparation of grid samples. Depending on the mechanisms of material processes to be identified from cryo-EM observation, the sampling process may be suitably simplified. For the purpose of mitigating beam damage, it may even be sufficient to prepare sample grids simply as dry states, where samples are deposited onto a TEM grid, dried, and then placed in liquid nitrogen prior to imaging.[63,64] In some cases, material structures exhibit differences between dry and solvated states,[154] which makes it necessary to observe solvated structures by freezing samples embedded within the solution. This can be performed with blotting procedures that produce a thin layer of frozen solvent on the grids, a process which may also be automated with vitrification machines that provides reproducibility.[33,155] Some samples require air-tight transfer, where an inert gas-filled glove box is used for producing the grids, and the grids are transferred to the holder in an air-tight container for imaging.[26,56] Combinations of glove-box and vitrification machines have been demonstrated earlier for the seamless transfer of samples within an Ar environment.[156] Methods for the transfer of samples in completely air-tight environments within different machines and ultimately to the TEM can be

useful for preserving structures of air-sensitive specimen. The emergence of frozen solution-state imaging with cryo-EM also necessitates the study of the properties of common solvents used in materials science processes under cryogenic conditions.[152] In particular, vitrification of non-aqueous solvents such as organic solvents or electrolytes are relatively less understood. Solvent composition impacts the stability of the free-standing frozen solution formed on the grids, as well as the extent of radiolysis which impacts image quality by the formation of radiolytic products.[152] Currently, beam induced radiolysis has been studied for many aqueous[33,157] solutions for biological applications, and more recently, for a few organic solvents.[158] A comprehensive study of a variety of solvents or liquids will benefit imaging materials at their solvated states.

Systems brought down to nanoscale models. The use of sample enclosures that encase nanoscale models of bulk processes is an alternative approach for preparing cryo-EM samples. These enclosures have been implemented extensively in liquid-phase transmission electron microscopy,[51] and are designed to seal the target material to protect it from drying out or reacting in ambient conditions, while keeping the assembly thin enough for TEM observation. For these purposes, materials used to encapsulate the samples should be electron beam-transparent and solvent impermeable. Graphene liquid cell enclosures encapsulate liquid with the sample, which would be sandwiched between two sheets of graphene (Fig. 7, top row). A demonstration of utilizing this graphene sandwiched structure has been performed for high-resolution imaging of solvated protein structures with cryo-EM.[159] Carbon film-based enclosures similarly encapsulate solvated samples with two sheets of ultrathin carbon that are a couple nanometers thick (Fig. 7, middle row). These enclosures have been beneficial in encapsulating and imaging wet samples such as biomaterials[160] or electrolytes.[161] In addition, microelectromechanical systems (MEMS) may be implemented to produce Si-based TEM sampling chips equipped with electron-transparent SiN_x windows, which encapsulates a nanometer-scale thick model system of a native working process within a designated spacer (Fig. 7, bottom row).[162] Once samples are encapsulated within these enclosures, they are cooled with a cryogen such as liquid nitrogen before being imaged with cryo-EM.

Optimizing instrumentation for materials science

For cryo-EM in structural biology, a revolutionary advancement that enabled the reconstruction of sub-nanometer-resolution 3D structures of proteins is the implementation of instruments dedicated to imaging biological materials. Examples include the direct electron detector,[163] the use of 300 kV acceleration voltage,[164] and the implementation of energy filters[165] and phase plates[166] to increase SNR and contrast for proteins embedded in vitreous ice. Additionally, developments in algorithms for dose-weighting[167] for extracting reliable data and pipelines for high-throughput data acquisition have made cryo-EM a standardized and widely-used technique in structural biology. The instrumentation available for imaging biological systems may be utilized for imaging materials with cryo-EM.
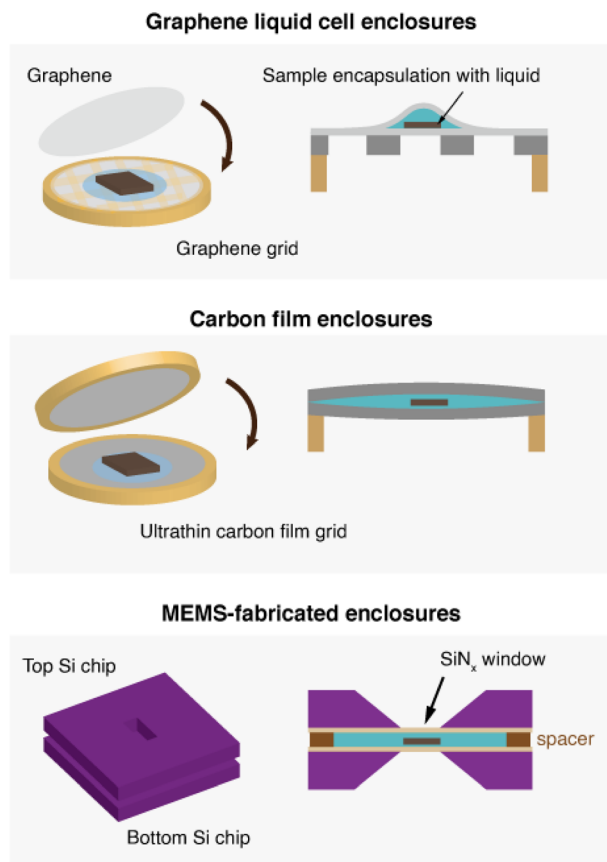
Fig. 7 Types of liquid cell enclosures that are used for encapsulating solvent and samples prior to cryogenic cooling to maintain solvated states. (Top) Graphene liquid cell enclosures, which involves the encapsulation of the sample and the surrounding solvent by sandwiching the sample between two sheets of graphene. (Middle) Carbon film enclosures, which encapsulates the sample and the solvent between two carbon grids. (Bottom) MEMS-fabricated enclosures made of Si chips and SiN_x windows, designated to seal liquids between two chips.

Incorporating cold field emission guns for high brightness, and direct electron detectors for increased SNR is beneficial for imaging beam-sensitive materials, retrieving maximum information from small electron doses. However, many cryo-TEM setups for structural biology are not optimized to meet the specific requirements of materials scientists.[57] One example is the need for spherical aberration (Cs) correction[48] which is crucial for high-resolution imaging for nanoscale materials— a feature typically not necessary for biological applications and thus often lacking in many cryo-TEM setups. Spherical aberration arises from inherent limitations in electron lenses, resulting in a significant reduction in point resolution. In images captured with an uncorrected microscope, spherical aberration causes a reversal in contrast beyond the resolution limit,[168] making accurate interpretation of the images challenging. For the resolution range used for images in high-resolution EM, Cs correction drastically improves the achievable resolution of the images.[169] Unfortunately, incorporating Cs correction into an

existing uncorrected cryo-EM setup is challenging as it requires substantial modifications to the electron column as well as specific operation protocols. To expand the use of cryo-EM in materials sciences, it would be highly beneficial to develop more cryo-EM setups specifically tailored for materials research. These setups could include conventional Cs-corrected microscopes with compatible cryo-transfer holders, or dedicated cryo-EMs incorporated with Cs correction. Additionally, as discussed with examples from mechanistic studies in battery chemistry and quantum materials, electron diffraction, STEM imaging and correlative elemental analysis techniques such as EDS or EELS are necessary in materials science but are not commonly used in structural biology. STEM, EDS, and EELS require installation of dedicated detectors. In addition to adding these detectors, techniques such as EELS can benefit from incorporating a monochromator to produce highly coherent electron beams to achieve higher spectral resolution.[170] Depending on the spectral resolution needed for imaging fine electronic structures with EELS, a monochromator for the electron beam may be useful.

TEM observation at cryogenic temperatures can be performed in two ways: by utilizing a dedicated cryogenic TEM equipped with a cryo-stage and an autoloader, or by using a cryogenic holder on a conventional TEM. A dedicated cryo-TEM is less versatile in terms of instrumentation but provides higher imaging stability, reducing drift or vibration from the external environment. For materials science purposes, using a cryogenic TEM holder may be a compelling option in many cases because it is versatile, economical, and more suitable for samples that undergo changes in ambient conditions. Additionally, commercial cryogenic holders have dual-axis tilt, which is crucial for aligning the desired crystallographic orientations in HRTEM. However, cryogenic holders suffer from more drift during imaging compared to a dedicated cryogenic stage, causing blurred images due to the boiling of the liquid nitrogen or vibrations from the external environment.[93,167] In addition, contaminants may be deposited during sample transfer within the cryogenic stations,[171] and automated imaging is more difficult to perform with the side-entry holder setup.

Software and hardware development for automated imaging for materials science may also be beneficial, especially for large-scale imaging to address heterogeneity.[172] This process involves acquiring images at low magnifications with minimal dose, and then designating locations to automatically image at high resolution, so the electron dose that the sample is exposed to is reduced. Currently, software is optimized to locate holes of holey support grids for data acquisition. Optimizing software to locate areas for imaging in materials systems using feature or contrast analysis could be implemented to achieve automated imaging for nanoscale materials.

In terms of sample preparation, setups that provide airtight environments are beneficial for imaging air-sensitive materials such as Li. Sampling procedures within an Ar environment in a glove box and methods to transport samples from one area to the next have been developed to minimize the exposure of sensitive samples to air. These are crucial

developments to maintain the integrity of the samples being imaged under cryo-EM.[163]

### Interpretation of data for obtaining mechanistic insights

A crucial aspect for utilizing cryo-EM for making conclusions in terms of mechanisms is to provide a reliable interpretation of data, mainly images, obtained from samples of interest.[47] A few necessary considerations before drawing conclusions from TEM data include understanding electron beam-induced effects, increasing signal-to-noise ratio (SNR), and implementing techniques to address data heterogeneity.

Benchmarking beam-induced effects. In solids, electron irradiation damage occurs through elastic scattering that includes atomic displacement and knock-on damage, and inelastic scattering that includes heating, radiolysis, and electrostatic charging.[173] While cryogenic temperatures enhance beam tolerance of the sample by mitigating effects from heating and radiolysis, elastic scattering effects such as atomic displacement and knock-on damage are still inevitable. These damage mechanisms manifest in materials by changes in

crystallinity of a sample,[174,175] shrinkage,[58] or defect formation.[176,177] Because of these structural changes during conventional, room temperature TEM, it was difficult to obtain high-resolution structures of beam sensitive materials. As shown by the beam damage experiment shown in Fig. 8a and b, Li dendrites exhibit visible damage from the electron beam when exposed to high electron dose rates during attempts at high-resolution imaging.[26] These qualitative changes show how beam damage is manifested in different samples, while also providing a method to estimate electron beam threshold. In the amorphous ice crystallization experiment shown in Fig. 8c and d, heating-induced crystallization shows significantly different features from beam-induced crystallization, suggesting that crystallization of amorphous ice from heat and the beam undergo different crystallization mechanisms.[136] These results indicate the necessity to probe and distinguish beam-induced artifacts from actual structures of samples.

One way to benchmark electron beam effects quantitatively is to utilize the intensity of crystalline peaks in the Fast Fourier Transform (FFT) of the images.[179] By obtaining sequential images of a material while undergoing electron beam-induced
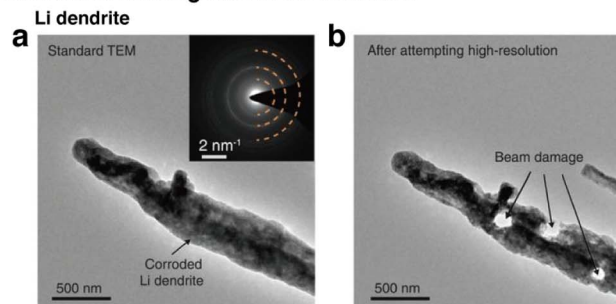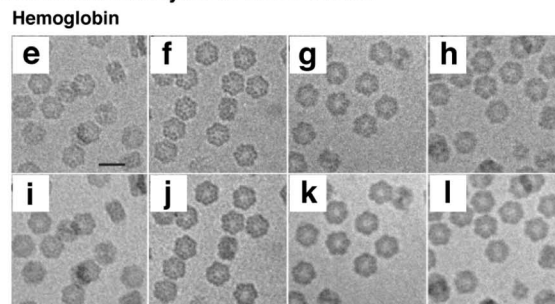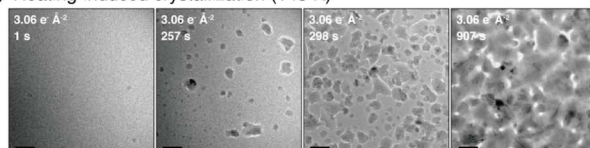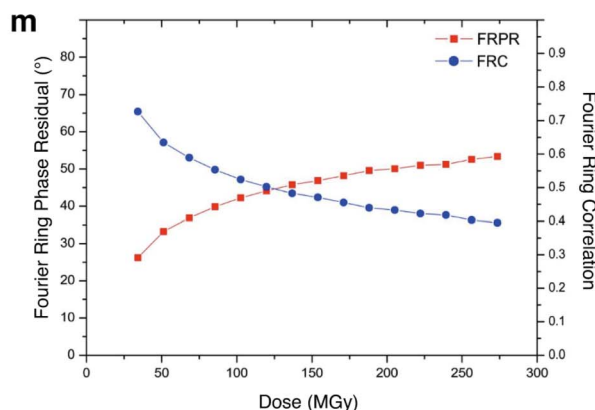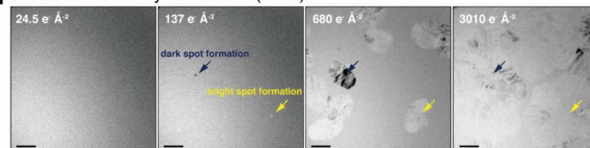

Fig. 8 Investigation and benchmarking of electron-beam effects on different samples. (a) Li dendrite image before high-resolution imaging attempt using conventional, room temperature TEM. (b) Li dendrite after beam damage caused by high electron doses after attempting high-resolution (reproduced with permission from ref. 26, copyright 2017 AAAS). (c) Example of heating-induced crystallization of ice, which is the intended process to be observed. (d) Example of beam-induced crystallization of ice from continuous irradiation, which produces artifacts that are different from the crystallization process observed by heating (reproduced with permission from ref. 136, copyright 2023 Nature Publishing Group). (e–l) Aligned and summed images of the protein hemoglobin embedded in vitreous ice, in which (a and e) are low-flux, (b and f) are medium-flux, (c and g) are high-flux, and (d and h) are high-flux short-exposure. (a–d) are 50 e Å^{-2} and (e–h) are 250 e Å^{-2}. (m) Plots of FRPR and FRC according to different dose rates calculated in MGy, providing information on the changes in low-resolution information according to accumulated dose. The threshold value of 45 deg for FRPR and 0.5 for FRC can be used to benchmark imaging dose rates (reproduced with permission from ref. 178, copyright 2011 IUCr Journals).

changes, one can gain insight into the effects that the beam poses on the crystallinity of the sample. Additionally, parameters such as the Fourier ring correlation (FRC), which indicates the highest reliable resolution of an image,[178] can be quantified as a function of cumulative dose. In an experiment for imaging the protein hemoglobin embedded in vitreous ice, the effects of cumulative dose and dose rates on the protein images have been shown (Fig. 8e–l). This data was quantified using the Fourier Ring Phase Residual (FRPR) and the FRC of images with different cumulative doses (Fig. 8m).[180] These parameters can be used to set a beam dose threshold with respect to the preservation of low-resolution structures. A value of 45° for the FRPR, and 0.5 for the FRC was used to benchmark the threshold of dose and to determine which images obtained are reliable for use. These dose-based image quantification methods have been utilized in structural biology to fully utilize information from images, giving more weight for reliability to the images that have had less exposure to the beam.[181]

Enhancement of signal-to-noise ratio. Due to the low beam tolerance for many materials imaged with cryo-EM, most imaging conditions are performed at low doses, which inevitably decreases the signal-to-noise ratio (SNR) of the images.[182] In structural biology, SNR is increased by averaging thousands of images of single proteins that exhibit the same projection, assuming that protein structures are homogeneous. However, in many nanomaterial systems, structures of each particle are heterogeneous, and therefore, strategies to denoise single images are desired. Denoising procedures for increasing SNR of single images have previously been developed for cryo-ET data, in which full utilization of each image is necessary.[183] While an approach to analyze the noise statistics and remove them accordingly may be useful, the noise in TEM images is signal-dependent, and are also correlated within rows and columns of pixels.[184] Deep learning-based methods were introduced to address signal-dependent noise for imaging. Since paired data for ground truth and noisy images are not available in most TEM experiments, self- and unsupervised methods are crucial to eliminate the need for training data.[183,185,186] Such methods were developed in biological cryo-EM where samples are mainly composed of light atoms and image contrast is inherently weak. Thus, application of these algorithms in the images from materials will be beneficial for retrieving accurate information.

Addressing heterogeneity. Many materials at the nanoscale exhibit high degrees of heterogeneity, making it challenging for TEM to capture all the different structures necessary to explain bulk-scale properties. For drawing consistent conclusions with these structural variabilities, it is important to be able to classify the structures and morphologies observed. In highly heterogeneous systems, acquiring a large number of images can aid in gathering significant statistical information on the nanoscale structures. The large-scale image acquisition process may be automated.[187] In terms of addressing sample heterogeneity, a relevant technique has been demonstrated for classifying highly heterogeneous shapes of exosomes.[172] After performing morphological segmentation of observed structures within the images using a trained neural network,[188] shape parameters can
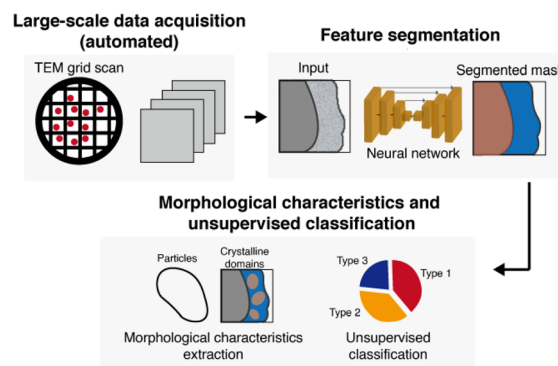

Fig. 9 Large-scale data acquisition and analysis for addressing heterogeneity in nanoscale structures. In this workflow, a sample of interest loaded on a TEM grid is scanned with automated imaging, acquiring a large number of images from multiple areas of the TEM grid to achieve a sufficient sample size. The large number of images are then fed through a neural network for segmentation of features. Then, depending on the features observed, morphological parameters can be extracted and classified using machine learning.

be quantified for the various morphologies or domains (Fig. 9). Machine learning-based algorithms, as extensively reviewed by Yao *et. al.*, can guide the process for obtaining consistent mechanistic insights from the many different structural forms observed.[189]

Because of the heterogeneous properties of nanoscale materials, imaging materials within their operational environment is particularly beneficial. 3D imaging with strategic sample preparation procedures, as demonstrated by An *et. al.* and Kalutantirige *et. al.*, have revealed how interactions with surrounding environments affect the structures and mechanisms within materials.[108,113] Tracking individual particles, as performed in ice crystallization observations,[135,136] is also beneficial for interpretation of data, as it directly visualizes structural effects within observed processes.

Conclusion and future outlook

In this Perspective, we have outlined the uses of cryo-EM for materials science, particularly in its role in revealing nanoscale mechanisms of complicated processes. In addition to the two-dimensional imaging of projections using the cryo-TEM and STEM modes, high-resolution imaging, correlative elemental analysis, three-dimensional imaging and time-resolved analysis have contributed vastly to providing more context behind mechanistic understanding of processes. Moreover, cryo-EM enables the observation of materials processes under conditions that reflect the native states, and with its use in conjunction with other correlative analytical techniques, it can reveal relationships between structural observations and mechanistic understanding. Currently, however, cryo-EM in use for elucidating mechanisms still require optimization in benchmarking such as quantification of beam-damage, or new approaches for producing thin samples. These challenges require additional improvements in cryo-sample preparation, instrumentation, and data interpretation, as we have outlined

in this Perspective. These enhancements will enable the novel studies of materials processes, while standardizing the use of cryo-EM as a tool for general use in materials science.

Data availability

No primary research results, software or code have been included and no new data were generated or analysed as part of this review.

Author contributions

M. L., Y. J., S. K., I. J., S. K., S.-H. J. and J. P. conceived and collaboratively drafted the manuscript.

Conflicts of interest

There are no conflicts to declare.

Acknowledgements

Notes and references

1 M. A. Pfeifer, G. J. Williams, I. A. Vartanyants, R. Harder and I. K. Robinson, *Nature*, 2006, **442**, 63–66.

2 M. Azubel, J. Koivisto, S. Malola, D. Bushnell, G. L. Hura, A. L. Koh, H. Tsunoyama, T. Tsukuda, M. Pettersson, H. Häkkinen and R. D. Kornberg, *Science*, 2014, **345**, 909–912.

3 B. H. Kim, J. Heo, S. Kim, C. F. Reboul, H. Chun, D. Kang, H. Bae, H. Hyun, J. Lim, H. Lee, B. Han, T. Hyeon, A. P. Alivisatos, P. Ercius, H. Elmlund and J. Park, *Science*, 2020, **368**, 60–67.

4 S. Jeon, T. Heo, S.-Y. Hwang, J. Ciston, K. C. Bustillo, B. W. Reed, J. Ham, S. Kang, S. Kim, J. Lim, K. Lim, J. S. Kim, M.-H. Kang, R. S. Bloom, S. Hong, K. Kim, A. Zettl, W. Y. Kim, P. Ercius, J. Park and W. C. Lee, *Science*, 2021, **371**, 498–503.

5 H. Wietfeldt, R. Meana-Pañeda, C. Machello, C. F. Reboul, C. T. S. Van, S. Kim, J. Heo, B. H. Kim, S. Kang, P. Ercius, J. Park and H. Elmlund, *Commun. Chem.*, 2024, **7**, 4.

6 M. A. Boles, D. Ling, T. Hyeon and D. V. Talapin, *Nat. Mater.*, 2016, **15**, 141–153.

7 A. H. Ip, S. M. Thon, S. Hoogland, O. Voznyy, D. Zhitomirsky, R. Debnath, L. Levina, L. R. Rollny, G. H. Carey, A. Fischer, K. W. Kemp, I. J. Kramer, Z. Ning, A. J. Labelle, K. W. Chou, A. Amassian and E. H. Sargent, *Nat. Nanotechnol.*, 2012, **7**, 577–582.

8 N. Kholmicheva, P. Moroz, H. Eckard, G. Jensen and M. Zamkov, *ACS Energy Lett.*, 2017, **2**, 154–160.

9 H. Park, H. Park, K. Song, S. H. Song, S. Kang, K. H. Ko, D. Eum, Y. Jeon, J. Kim, W. M. Seong, H. Kim, J. Park and K. Kang, *Nat. Chem.*, 2022, **14**, 614–622.

10 D. Eum, S. O. Park, H. Y. Jang, Y. Jeon, J. H. Song, S. Han, K. Kim and K. Kang, *Nat. Mater.*, 2024, **23**, 1093–1099.

11 M. Tang, H. Yan, X. Zhang, Z. Zheng and S. Chen, *Adv. Mater.*, 2023, 2306387.

12 R. Sun, Z. Xia, X. Xu, R. Deng, S. Wang and G. Sun, *Nano Energy*, 2020, **75**, 104919.

13 F. C. Cetinbas, R. K. Ahluwalia, N. N. Kariuki and D. J. Myers, *J. Electrochem. Soc.*, 2018, **165**, F1051–F1058.

14 S. Kim, J. Kwag, C. Machello, S. Kang, J. Heo, C. F. Reboul, D. Kang, S. Kang, S. Shim, S. J. Park, B. H. Kim, T. Hyeon, P. Ercius, H. Elmlund and J. Park, *Nano Lett.*, 2021, **21**, 1175–1183.

15 J. Kim, A. Park, J. Kim, S. J. Kwak, J. Y. Lee, D. Lee, S. Kim, B. K. Choi, S. Kim, J. Kwag, Y. Kim, S. Jeon, W. C. Lee, T. Hyeon, C. H. Lee, W. B. Lee and J. Park, *Adv. Mater.*, 2022, **34**, 2206066.

16 M. H. Kang, J. Park, S. Kang, S. Jeon, M. Lee, J. Y. Shim, J. Lee, T. J. Jeon, M. K. Ahn, S. M. Lee, O. Kwon, B. H. Kim, J. R. Meyerson, M. J. Lee, K. Il Lim, S. H. Roh, W. C. Lee and J. Park, *Adv. Mater.*, 2021, **33**, 2102991.

17 M. C. Weidman, D. M. Smilgies and W. A. Tisdale, *Nat. Mater.*, 2016, **15**, 775–781.

18 L. Houben, H. Weissman, S. G. Wolf and B. Rybtchinski, *Nature*, 2020, **579**, 540–543.

19 A. McPherson, *Methods Mol. Biol.*, 2017, **1607**, 17–50.

20 J. S. Du, Y. Bae and J. J. De Yoreo, *Nat. Rev. Mater.*, 2024, **9**, 229–248.

21 E. B. Moore and V. Molinero, *Phys. Chem. Chem. Phys.*, 2011, **13**, 20008–20016.

22 R. S. Smith, C. Huang, E. K. L. Wong and B. D. Kay, *Surf. Sci. Lett.*, 1996, **367**, L13–L18.

23 H. Baek, S. Kang, J. Heo, S. Choi, R. Kim, K. Kim, N. Ahn, Y. G. Yoon, T. Lee, J. B. Chang, K. S. Lee, Y. G. Park and J. Park, *Nat. Commun.*, 2024, **15**, 1671.

24 G. Zhu, M. L. Sushko, J. S. Loring, B. A. Legg, M. Song, J. A. Soltis, X. Huang, K. M. Rosso and J. J. De Yoreo, *Nature*, 2021, **590**, 416–422.

25 D. Jacobsson, F. Panciera, J. Tersoff, M. C. Reuter, S. Lehmann, S. Hofmann, K. A. Dick and F. M. Ross, *Nature*, 2016, **531**, 317–322.

26 Y. Li, Y. Li, A. Pei, K. Yan, Y. Sun, C.-L. Wu, L.-M. Joubert, R. Chin, A. L. Koh, Y. Yu, J. Perrino, B. Butz, S. Chu and Y. Cui, *Science*, 2017, **358**, 506–510.

27 E. Trevisanello, R. Ruess, G. Conforto, F. H. Richter and J. Janek, *Adv. Energy Mater.*, 2021, **11**, 2003400.

28 C. Kirsch, C. Dreßler and D. Sebastiani, *J. Phys. Chem. C*, 2022, **126**, 12136–12149.

29 X. Wang, J. Li and Q. Chen, *Matter*, 2023, **6**, 2488–2612.

30 D. Li, Q. Chen, J. Chun, K. Fichthorn, J. De Yoreo and H. Zheng, *Chem. Rev.*, 2023, **123**, 3127–3159.

31 Y. Cheng, *Cell*, 2015, **161**, 450–457.

32 M. C. Darrow, J. P. Moore, R. J. Walker, K. Doering and R. S. King, *Microsc. Microanal.*, 2019, **25**, 994–995.

33 G. Weissenberger, R. J. M. Henderikx and P. J. Peters, *Nat. Methods*, 2021, **18**, 463–471.

34 V. P. Dandey, W. C. Budell, H. Wei, D. Bobe, K. Maruthi, M. Kopylov, E. T. Eng, P. A. Kahn, J. E. Hinshaw, N. Kundu, C. M. Nimigean, C. Fan, N. Sukomon, S. A. Darst, R. M. Saecker, J. Chen, B. Malone, C. S. Potter and B. Carragher, *Nat. Methods*, 2020, **17**, 897–900.

35 S. Wu, J. P. Armache and Y. Cheng, *Microscopy*, 2016, **65**, 35–41.

36 X. Li, P. Mooney, S. Zheng, C. R. Booth, M. B. Braunfeld, S. Gubbens, D. A. Agard and Y. Cheng, *Nat. Methods*, 2013, **10**, 584–590.

37 A. Punjani, J. L. Rubinstein, D. J. Fleet and M. A. Brubaker, *Nat. Methods*, 2017, **14**, 290–296.

38 E. D. Zhong, T. Bepler, B. Berger and J. H. Davis, *Nat. Methods*, 2021, **18**, 176–185.

39 J. L. Vilas, J. M. Carazo and C. O. S. Sorzano, *Chem. Rev.*, 2022, **122**, 13915–13951.

40 S. Q. Zheng, E. Palovcak, J. P. Armache, K. A. Verba, Y. Cheng and D. A. Agard, *Nat. Methods*, 2017, **14**, 331–332.

41 A. L. Parry, P. H. H. Bomans, S. J. Holder, N. A. J. M. Sommerdijk and S. C. G. Biagini, *Angew. Chem., Int. Ed.*, 2008, **47**, 8859–8862.

42 K. Mortensenf and Y. Talmon, *Macromolecules*, 1995, **28**, 8829–8834.

43 Y. He, Z. Li, P. Simone and T. P. Lodge, *J. Am. Chem. Soc.*, 2006, **128**, 2745–2750.

44 R. Zana and Y. Talmon, *Nature*, 1993, **362**, 228–230.

45 V. A. Davis, A. N. G. Parra-Vasquez, M. J. Green, P. K. Rai, N. Behabtu, V. Prieto, R. D. Booker, J. Schmidt, E. Kesselman, W. Zhou, H. Fan, W. W. Adams, R. H. Hauge, J. E. Fischer, Y. Cohen, Y. Talmon, R. E. Smalley and M. Pasquali, *Nat. Nanotechnol.*, 2009, **4**, 830–834.

46 X. C. Ren, X. Q. Zhang, R. Xu, J. Q. Huang and Q. Zhang, *Adv. Mater.*, 2020, **32**, 1908293.

47 Y. Li, W. Huang, Y. Li, W. Chiu and Y. Cui, *ACS Nano*, 2020, **14**, 9263–9276.

48 S. Kang, J. Cha, Y. S. Jo, Y. J. Lee, H. Sohn, Y. Kim, C. K. Song, Y. Kim, D. H. Lim, J. Park and C. W. Yoon, *Adv. Mater.*, 2023, **35**, 2203364.

49 Y. Kim, S. Kang, D. Kang, K. R. Lee, C. K. Song, J. Sung, J. S. Kim, H. Lee, J. Park and J. Yi, *Angew. Chem., Int. Ed.*, 2021, **60**, 25411–25418.

50 M. V. Kovalenko, L. Manna, A. Cabot, Z. Hens, D. V. Talapin, C. R. Kagan, V. I. Klimov, A. L. Rogach, P. Reiss, D. J. Milliron, P. Guyot-Sionnnest, G. Konstantatos, W. J. Parak, T. Hyeon, B. A. Korgel, C. B. Murray and W. Heiss, *ACS Nano*, 2015, **9**, 1012–1057.

51 J. Kim, S. Kang, F. Cheng, Y. Wang, X. Ye and J. Park, *MRS Bull.*, 2024, **49**, 365–376.

52 H. Wu, H. Friedrich, J. P. Patterson, N. A. J. M. Sommerdijk and N. de Jonge, *Adv. Mater.*, 2020, **32**, 2001582.

53 R. F. Egerton, P. Li and M. Malac, *Micron*, 2004, **35**, 399–409.

54 L. Liu, D. Zhang, Y. Zhu and Y. Han, *Commun. Chem.*, 2020, **3**, 99.

55 Y. Li, W. Huang, Y. Li, A. Pei, D. T. Boyle and Y. Cui, *Joule*, 2018, **2**, 2167–2177.

56 X. Wang, Y. Li and Y. S. Meng, *Joule*, 2018, **2**, 2225–2234.

57 R. E. A. Williams, D. W. Mccomb and S. Subramaniam, *MRS Bull.*, 2019, **44**, 929–934.

58 R. F. Egerton, *Micron*, 2019, **119**, 72–87.

59 G. T. Oostergetel, F. J. Esselink and G. Hadziioannou, *Langmuir*, 1995, **11**, 3721–3724.

60 M. J. M. Wirix, P. H. H. Bomans, H. Friedrich, N. A. J. M. Sommerdijk and G. De With, *Nano Lett.*, 2014, **14**, 2033–2038.

61 K. Steinberg, X. Yuan, C. K. Klein, N. Lazouski, M. Mecklenburg, K. Manthiram and Y. Li, *Nat. Energy*, 2023, **8**, 138–148.

62 E. Zhang, M. Mecklenburg, X. Yuan, C. Wang, B. Liu and Y. Li, *iScience*, 2022, **22**, 105689.

63 F. Banihashemi, G. Bu, A. Thaker, D. Williams, J. Y. S. Lin and B. L. Nannenga, *Ultramicroscopy*, 2020, **216**, 113048.

64 Y. Li, K. Wang, W. Zhou, Y. Li, R. Vila, W. Huang, H. Wang, G. Chen, G. H. Wu, Y. Tsao, H. Wang, R. Sinclair, W. Chiu and Y. Cui, *Matter*, 2019, **1**, 428–438.

65 Y. Kim, J. Sung, S. Kang, J. Lee, M. H. Kang, S. Hwang, H. Park, J. Kim, Y. Kim, E. Lee, G. S. Park, D. H. Kim and J. Park, *J. Mater. Chem. A*, 2021, **9**, 19796–19806.

66 E. J. Vandenbussche, C. P. Clark, R. J. Holmes and D. J. Flannigan, *ACS Omega*, 2020, **5**, 31867–31871.

67 L. Bao, P. Gao, T. Song, F. Xu, Z. Li and G. Xu, *Crystals*, 2023, **13**, 973.

68 B. Yuan and Y. Yu, *Chem*, 2022, **8**, 327–339.

69 N. Dumaresq, N. Brodusch, S. Bessette and R. Gauvin, *Ultramicroscopy*, 2024, **262**, 113977.

70 H. Tan, J. Verbeeck, A. Abakumov and G. Van Tendeloo, *Ultramicroscopy*, 2012, **116**, 24–33.

71 Z. Luo, X. Qiu, C. Liu, S. Li, C. Wang, G. Zou, H. Hou and X. Ji, *Nano Energy*, 2021, **79**, 105507.

72 X. B. Cheng, R. Zhang, C. Z. Zhao and Q. Zhang, *Chem. Rev.*, 2017, **117**, 10403–10473.

73 X. Yuan, B. Liu, M. Mecklenburg and Y. Li, *Nature*, 2023, **620**, 86–91.

74 W. Liu, P. Liu and D. Mitlin, *Adv. Energy Mater.*, 2020, **10**, 2002297.

75 E. Peled and S. Menkin, *J. Electrochem. Soc.*, 2017, **164**, A1703–A1719.

76 H. Park, Y. Jeon, M. Park, I. Jung, J. Shin, Y. Kim, W. K. Kim, K. H. Ryu, W. B. Lee and J. Park, *ACS Nano*, 2024, **18**, 12885–12896.

77 Y. Gao, T. Rojas, K. Wang, S. Liu, D. Wang, T. Chen, H. Wang, A. T. Ngo and D. Wang, *Nat. Energy*, 2020, **5**, 534–542.

78 M. J. Zachman, Z. Tu, S. Choudhury, L. A. Archer and L. F. Kourkoutis, *Nature*, 2018, **560**, 345–349.

79 N. S. Dutta, P. J. Weddle, O. Hathaway, M. Al-Jassim and K. Jungjohann, *ACS Energy Lett.*, 2024, **9**, 2464–2471.

80 J. Quinn, B. Wu, Y. Xu, M. H. Engelhard, J. Xiao and C. Wang, *ACS Nano*, 2022, **16**, 21063–21070.

81 H. Park, Y. Jeon, W. J. Chung, Y. Bae, J. Kim, H. Baek and J. Park, *ACS Energy Lett.*, 2023, **8**, 715–721.

82 C. Fang, J. Li, M. Zhang, Y. Zhang, F. Yang, J. Z. Lee, M. H. Lee, J. Alvarado, M. A. Schroeder, Y. Yang, B. Lu, N. Williams, M. Ceja, L. Yang, M. Cai, J. Gu, K. Xu, X. Wang and Y. S. Meng, *Nature*, 2019, **572**, 511–515.

83 B. Han, X. Li, Q. Wang, Y. Zou, G. Xu, Y. Cheng, Z. Zhang, Y. Zhao, Y. Deng, J. Li and M. Gu, *Adv. Mater.*, 2021, **34**, 2108252.

84 X. Wang, M. Zhang, J. Alvarado, S. Wang, M. Sina, B. Lu, J. Bouwer, W. Xu, J. Xiao, J. G. Zhang, J. Liu and Y. S. Meng, *Nano Lett.*, 2017, **17**, 7606–7612.

85 Y. Liu, D. Lin, Y. Li, G. Chen, A. Pei, O. Nix, Y. Li and Y. Cui, *Nat. Commun.*, 2018, **9**, 3656.

86 K. Dong, Y. Xu, J. Tan, M. Osenberg, F. Sun, Z. Kochovski, D. T. Pham, S. Mei, A. Hilger, E. Ryan, Y. Lu, J. Banhart and I. Manke, *ACS Energy Lett.*, 2021, **6**, 1719–1728.

87 B. Zhang, H. Shi, Z. Ju, K. Huang, C. Lian, Y. Wang, O. Sheng, J. Zheng, J. Nai, T. Liu, Y. Jin, Y. Liu, C. J. Zhang and X. Tao, *J. Mater. Chem. A*, 2020, **8**, 26045–26054.

88 Y. Xu, H. Jia, P. Gao, D. E. Galvez-Aranda, S. P. Beltran, X. Cao, P. M. L. Le, J. Liu, M. H. Engelhard, S. Li, G. Ren, J. M. Seminario, P. B. Balbuena, J. G. Zhang, W. Xu and C. Wang, *Nat. Energy*, 2023, **8**, 1345–1354.

89 Y. Yang, Y. Yin, D. M. Davies, M. Zhang, M. Mayer, Y. Zhang, E. S. Sablina, S. Wang, J. Z. Lee, O. Borodin, C. S. Rustomji and Y. S. Meng, *Energy Environ. Sci.*, 2020, **13**, 2209–2219.

90 D. T. Boyle, W. Huang, H. Wang, Y. Li, H. Chen, Z. Yu, W. Zhang, Z. Bao and Y. Cui, *Nat. Energy*, 2021, **6**, 487–494.

91 X. Xing, Y. Li, X. Wang, V. Petrova, H. Liu and P. Liu, *Energy Storage Mater.*, 2019, **21**, 474–480.

92 Y. Zhu, *Acc. Chem. Res.*, 2021, **54**, 3518–3528.

93 E. Bianco and L. F. Kourkoutis, *Acc. Chem. Res.*, 2021, **54**, 3277–3287.

94 Y. Zhu, A. R. Moodenbaugh, Z. X. Cai, J. Tafto, M. Suenaga and D. O. Welch, *Phys. Rev. Lett.*, 1994, **73**, 3026.

95 P. Moradifar, Y. Liu, J. Shi, M. L. Siukola Thurston, H. Utzat, T. B. van Driel, A. M. Lindenberg and J. A. Dionne, *Chem. Rev.*, 2023, **123**, 12757–12794.

96 B. H. Savitzky, I. El Baggari, C. B. Clement, E. Waite, B. H. Goodge, D. J. Baek, J. P. Sheckelton, C. Pasco, H. Nair, N. J. Schreiber, J. Hoffman, A. S. Admasu, J. Kim, S. W. Cheong, A. Bhattacharya, D. G. Schlom, T. M. McQueen, R. Hovden and L. F. Kourkoutis, *Ultramicroscopy*, 2018, **191**, 56–65.

97 I. El Baggari, N. Sivadas, G. M. Stiehl, J. Waelder, D. C. Ralph, C. J. Fennie and L. F. Kourkoutis, *Phys. Rev. Lett.*, 2020, **125**, 165302.

98 I. El Baggari, D. J. Baek, M. J. Zachman, D. Lu, Y. Hikita, H. Y. Hwang, E. A. Nowadnick and L. F. Kourkoutis, *Nat. Commun.*, 2021, **12**, 3747.

99 B. H. Goodge, B. H. Goodge, E. Bianco, N. Schnitzer, H. W. Zandbergen, H. W. Zandbergen, L. F. Kourkoutis and L. F. Kourkoutis, *Microsc. Microanal.*, 2020, **26**, 439–446.

100 B. H. Goodge, D. J. Baek and L. F. Kourkoutis, *arXiv*, 2020, preprint arxiv: 2007.09747, DOI: 10.48550/arXiv.2007.09747.

101 X. He, R. Kostin, E. Knight, M. G. Han, J. Mun, I. Bozovic, C. Jing and Y. Zhu, *Ultramicroscopy*, 2024, **267**, 114037.

102 B. Plotkin-Swing, A. Mittelberger, B. Haas, J. C. Idrobo, B. Graner, N. Dellby, M. T. Hotz, C. E. Meyer, S. C. Quillin, O. L. Krivanek and T. C. Lovejoy, *Microsc. Microanal.*, 2023, **29**, 1698–1699.

103 A. J. Silvaroli, T. R. Heyl, M. Chyasnavichyus, J. M. Beebe, D. Ahn, S. Mangold, Q. Chen, M. Wang and K. R. Shull, *Macromolecules*, 2023, **56**, 4075–4086.

104 C. A. Ron, K. Vanness, A. Rasmuson and W. P. Johnson, *Environ. Sci.:Nano*, 2019, **6**, 1921–1931.

105 J. Lee, S. Kang, E. Lee, M. Kang, J. Sung, T. J. Kim, P. Christopher, J. Park and D. H. Kim, *J. Mater. Chem. A*, 2022, **10**, 7029–7035.

106 C. Galeano, J. C. Meier, V. Peinecke, H. Bongard, I. Katsounaros, A. A. Topalov, A. Lu, K. J. J. Mayrhofer and F. Schüth, *J. Am. Chem. Soc.*, 2012, **134**, 20457–20465.

107 R. Girod, T. Lazaridis, H. A. Gasteiger and V. Tileli, *Nat. Catal.*, 2023, **6**, 383–391.

108 H. An, J. W. Smith, B. Ji, S. Cotty, S. Zhou, L. Yao, F. C. Kalutantirige, W. Chen, Z. Ou, X. Su, J. Feng and Q. Chen, *Sci. Adv.*, 2022, **8**, eabk1888.

109 Y. Li, Z. Wu, C. Wang, X. Yu, W. Gao, B. Wang, C. Wu, Y. Yao, J. Yang and Z. Zou, *Adv. Funct. Mater.*, 2024, **34**, 2310428.

110 S. Ott, A. Orfanidi, H. Schmies, B. Anke, H. N. Nong, J. Hübner, U. Gernert, M. Gliech, M. Lerch and P. Strasser, *Nat. Mater.*, 2020, **19**, 77–85.

111 M. Lopez-Haro, L. Guétaz, T. Printemps, A. Morin, S. Escribano, P. H. Jouneau, P. Bayle-Guillemaud, F. Chandezon and G. Gebel, *Nat. Commun.*, 2014, **5**, 5229.

112 K. Yu, J. L. Hart, J. Xie, M. L. Taheri and P. Ferreira, *Nano Energy*, 2023, **111**, 108393.

113 F. C. Kalutantirige, J. He, L. Yao, S. Cotty, S. Zhou, J. W. Smith, E. Tajkhorshid, C. M. Schroeder, J. S. Moore, H. An, X. Su, Y. Li and Q. Chen, *Nat. Commun.*, 2024, **15**, 2852.

114 J. P. Patterson, Y. Xu, M. A. Moradi, N. A. J. M. Sommerdijk and H. Friedrich, *Acc. Chem. Res.*, 2017, **50**, 1495–1501.

115 Z. Chen, K. Higashi, K. Ueda and K. Moribe, *Nano Lett.*, 2022, **22**, 6841–6846.

116 J. J. De Yoreo, P. U. P. A. Gilbert, N. A. J. M. Sommerdijk, R. L. Penn, S. Whitelam, D. Joester, H. Zhang, J. D. Rimer, A. Navrotsky, J. F. Banfield, A. F. Wallace, F. M. Michel, F. C. Meldrum, H. Cölfen and P. M. Dove, *Science*, 2015, **349**, aaa6760.

117 Y. Tsarfati, S. Rosenne, H. Weissman, L. J. W. Shimon, D. Gur, B. A. Palmer and B. Rybtchinski, *ACS Cent. Sci.*, 2018, **4**, 1031–1036.

118 A. Dey, P. H. H. Bomans, F. A. Müller, J. Will, P. M. Frederik, G. De With and N. A. J. M. Sommerdijk, *Nat. Mater.*, 2010, **9**, 1010–1014.

119 B. P. Pichon, P. H. H. Bomans, P. M. Frederik and N. A. J. M. Sommerdijk, *J. Am. Chem. Soc.*, 2008, **130**, 4034–4040.

120 E. M. Pouget, P. H. H. Bomans, J. A. C. M. Goos, P. M. Frederik, G. De With and N. A. J. M. Sommerdijk, *Science*, 2009, **323**, 1455–1458.

121 J. J. De Yoreo and N. A. J. M. Sommerdijk, *Nat. Rev. Mater.*, 2016, **1**, 16035.

122 A. F. Ogata, A. M. Rakowski, B. P. Carpenter, D. A. Fishman, J. G. Merham, P. J. Hurst and J. P. Patterson, *J. Am. Chem. Soc.*, 2020, **142**, 1433–1442.

123 L. He, H. K. Hsu, L. Li, L. T. Lin, T. H. Tu, T. G. Ong, G. G. Liou and Y. T. Chan, *Chem*, 2022, **8**, 494–507.

124 F. Wang, O. Gnewou, A. Solemanifar, V. P. Conticello and E. H. Egelman, *Chem. Rev.*, 2022, **122**, 14055–14065.

125 L. Kang, A. Chao, M. Zhang, T. Yu, J. Wang, Q. Wang, H. Yu, N. Jiang and D. Zhang, *J. Am. Chem. Soc.*, 2021, **143**, 5890–5902.

126 A. E. S. Van Driessche, N. Van Gerven, R. R. M. Joosten, W. L. Ling, M. Bacia, N. Sommerdijk and M. Sleutel, *Nat. Commun.*, 2021, **12**, 3902.

127 L. Ziserman, H. Y. Lee, S. R. Raghavan, A. Mor and D. Danino, *J. Am. Chem. Soc.*, 2011, **133**, 2511–2517.

128 C. Lei, Y. H. Wang, P. X. Zhuang, Y. T. Li, Q. Q. Wan, Y. X. Ma, F. R. Tay and L. N. Niu, *J. Dent. Res.*, 2022, **101**, 505–514.

129 M. Armstrong, B.-G. Han, S. Gomez, J. Turner, D. A. Fletcher and R. M. Glaeser, *Biophys. J.*, 2020, **118**, 708–719.

130 S. Y. Schmid, K. Lachowski, H. T. Chiang, L. Pozzo, J. De Yoreo and S. Zhang, *Angew. Chem., Int. Ed.*, 2023, **62**, e202309725.

131 J. P. Patterson, M. P. Robin, C. Chassenieux, O. Colombani and R. K. O'Reilly, *Chem. Soc. Rev.*, 2014, **43**, 2412–2425.

132 E. Sutter, P. Sutter, A. V. Tkachenko, R. Krahne, J. De Graaf, M. Arciniegas and L. Manna, *Nat. Commun.*, 2016, **7**, 11213.

133 G. P. Johari, *Philos. Mag. B*, 1998, **78**, 375–383.

134 L. Lupi, A. Hudait, B. Peters, M. Grünwald, R. Gotchy Mullen, A. H. Nguyen and V. Molinero, *Nature*, 2017, **551**, 218–222.

135 X. Huang, L. Wang, K. Liu, L. Liao, H. Sun, J. Wang, X. Tian, Z. Xu, W. Wang, L. Liu, Y. Jiang, J. Chen, E. Wang and X. Bai, *Nature*, 2023, **617**, 86–91.

136 M. Lee, S. Y. Lee, M. H. Kang, T. K. Won, S. Kang, J. Kim, J. Park and D. J. Ahn, *Nat. Commun.*, 2024, **15**, 908.

137 C. R. Krüger, N. J. Mowry, G. Bongiovanni, M. Drabbels and U. J. Lorenz, *Nat. Commun.*, 2023, **14**, 2812.

138 C. R. Krüger, N. J. Mowry, M. Drabbels and U. J. Lorenz, *J. Phys. Chem. Lett.*, 2024, **15**, 4244–4248.

139 T. L. Malkin, B. J. Murray, C. G. Salzmann, V. Molinero, S. J. Pickering and T. F. Whale, *Phys. Chem. Chem. Phys.*, 2015, **17**, 60–76.

140 W. F. Kuhs, C. Sippel, A. Falenty and T. C. Hansen, *Proc. Natl. Acad. Sci. U.S.A.*, 2012, **109**, 21259–21264.

141 J. Lee, S. Y. Lee, D. K. Lim, D. J. Ahn and S. Lee, *J. Am. Chem. Soc.*, 2019, **141**, 18682–18693.

142 C. Lee, Y. Lee, W. H. Jung, T.-Y. Kim, T. Kim, D.-N. Kim and D. J. Ahn, *Sci. Adv.*, 2022, **8**, 185.

143 S. Y. Lee, M. Kim, T. K. Won, S. H. Back, Y. Hong, B. Kim and D. J. Ahn, *Nat. Commun.*, 2022, **13**, 6532.

144 U. J. Lorenz, *Curr. Opin. Struct. Biol.*, 2024, **87**, 102840.

145 O. F. Harder, S. V. Barrass, M. Drabbels and U. J. Lorenz, *Nat. Commun.*, 2023, **14**, 5649.

146 L. Rutten, M. de Beer, R. Roverts, E. M. Sánchez and N. Sommerdijk, *Microsc. Microanal.*, 2023, **29**, 1935–1936.

147 A. P. Conlan, E. Tillotson, A. Rakowski, D. Cooper and S. J. Haigh, *J. Microsc.*, 2020, **279**, 168–176.

148 V. Lam and E. Villa, in *Methods in Molecular Biology*, Humana Press Inc., USA, 2021, vol. 2215, pp. 49–82.

149 X. Zhang, Z. Guo, X. Li, Q. Liu, H. Hu, F. Li, Q. Huang, L. Zhang, Y. Tang and J. Huang, *Energy Environ. Sci.*, 2024, **17**, 1436–1447.

150 D. Chmielewski, M. F. Schmid, G. Simmons, J. Jin and W. Chiu, *Nat. Microbiol.*, 2022, **7**, 1270–1279.

151 R. A. Woldeyes, M. Nishiga, A. S. Vander Roest, L. Engel, P. Giri, G. C. Montenegro, A. C. Wu, A. R. Dunn, J. A. Spudich, D. Bernstein, M. F. Schmid, J. C. Wu and W. Chiu, *bioRxiv*, 2023, DOI: 10.1101/2023.10.26.564098.

152 A. Matatyaho Ya'Akobi and Y. Talmon, *Acc. Chem. Res.*, 2021, **54**, 2100–2109.

153 H. Koh, E. Detsi and E. A. Stach, *Microsc. Microanal.*, 2023, **29**, 1350–1356.

154 Z. Zhang, Y. Li, R. Xu, W. Zhou, Y. Li, S. T. Oyakhire, Y. Wu, J. Xu, H. Wang, Z. Yu, D. T. Boyle, W. Huang, Y. Ye, H. Chen, J. Wan, Z. Bao, W. Chiu and Y. Cui, *Science*, 2022, **375**, 66–70.

155 R. B. G. Ravelli, F. J. T. Nijpels, R. J. M. Henderikx, G. Weissenberger, S. Thewessem, A. Gijsbers, B. Beulen, C. López-Iglesias and P. J. Peters, *Nat. Commun.*, 2020, **11**, 2563.

156 M. R. Vos, P. H. H. Bomans, P. M. Frederik and N. A. J. M. Sommerdijk, *Ultramicroscopy*, 2008, **108**, 1478–1483.

157 J. Dubochet, J. Lepault, R. Freeman, J. A. Berriman and J. -C. Homo, *J. Microsc.*, 1982, **128**, 219–237.

158 P. Zhang, H. Du, S. Cui, P. Zhou and Y. Xu, *Responsive Mater.*, 2023, **1**, e20230025.

159 J. Xu, X. Gao, L. Zheng, X. Jia, K. Xu, Y. Ma, X. Wei, N. Liu, H. Peng and H. W. Wang, *Proc. Natl. Acad. Sci. U. S. A.*, 2024, **121**, e2309384121.

160 L. Kong, J. Liu, M. Zhang, Z. Lu, H. Xue, A. Ren, J. Liu, J. Li, W. L. Ling and G. Ren, *Nat. Commun.*, 2023, **14**, 5641.

161 Y. Xie, J. Wang, B. H. Savitzky, Z. Chen, Y. Wang, S. Betzler, K. Bustillo, K. Persson, Y. Cui, L.-W. Wang, C. Ophus, P. Ercius and H. Zheng, *Sci. Adv.*, 2023, **9**, eadc9721.

162 Y. Son, B. H. Kim, B. K. Choi, Z. Luo, J. Kim, G. H. Kim, S. J. Park, T. Hyeon, S. Mehraeen and J. Park, *ACS Appl. Mater. Interfaces*, 2022, **14**, 22810–22817.

163 G. McMullan, A. R. Faruqi and R. Henderson, in *Methods Enzymol.*, Academic Press Inc., USA, 2016, vol. 579, pp. 1–17.

164 K. Neselu, B. Wang, W. J. Rice, C. S. Potter, B. Carragher and E. Y. D. Chua, *J. Struct. Biol. X*, 2023, **7**, 100085.

165 T. Nakane, A. Kotecha, A. Sente, G. McMullan, S. Masiulis, P. M. G. E. Brown, I. T. Grigoras, L. Malinauskaite, T. Malinauskas, J. Miehling, T. Uchański, L. Yu, D. Karia, E. V. Pechnikova, E. de Jong, J. Keizer, M. Bischoff,

J. McCormack, P. Tiemeijer, S. W. Hardwick, D. Y. Chirgadze, G. Murshudov, A. R. Aricescu and S. H. W. Scheres, *Nature*, 2020, **587**, 152–156.

166 R. Danev and W. Baumeister, *Curr. Opin. Struct. Biol.*, 2017, **46**, 87–94.

167 Y. Kayama, R. N. Burton-Smith, C. Song, N. Terahara, T. Kato and K. Murata, *Sci. Rep.*, 2021, **11**, 8395.

168 C. Hetherington, *Mater. Today*, 2004, **7**, 50–55.

169 N. Tanaka, *Sci. Technol. Adv. Mater.*, 2008, **9**, 014111.

170 N. D. Browning, I. Arslan, R. Erni, J. C. Idrobo, A. Ziegler, J. Bradley, Z. Dai, E. A. Stach and A. Bleloch, *J. Phys.: Conf. Ser.*, 2006, **26**, 59.

171 K. Sader, R. Matadeen, P. Castro Hartmann, T. Halsan and C. Schlichten, *Acta Crystallogr., Sect. D:Struct. Biol.*, 2020, **76**, 313–325.

172 K. S. Kapoor, S. Kong, H. Sugimoto, W. Guo, V. Boominathan, Y. L. Chen, S. L. Biswal, T. Terlier, K. M. McAndrews and R. Kalluri, *ACS Nano*, 2024, **18**, 11717–11731.

173 D. Cheng, B. Lu, G. Raghavendran, M. Zhang and Y. S. Meng, *Matter*, 2022, **5**, 26–42.

174 H. Ma, D. Kim, S. I. Park, B. K. Choi, G. Park, H. Baek, H. Lee, H. Kim, J. S. Yu, W. C. Lee, J. Park and J. Yang, *Adv. Sci.*, 2023, **10**, 2205690.

175 M. U. Rothmann, W. Li, Y. Zhu, A. Liu, Z. Ku, U. Bach, J. Etheridge and Y. B. Cheng, *Adv. Mater.*, 2018, **30**, 1800629.

176 O. Dyck, S. Kim, S. V. Kalinin and S. Jesse, *Appl. Phys. Lett.*, 2017, **111**, 113104.

177 H. Malekpour, P. Ramnani, S. Srinivasan, G. Balasubramanian, D. L. Nika, A. Mulchandani, R. K. Lake and A. A. Balandin, *Nanoscale*, 2016, **8**, 14608–14616.

178 W. Zhao, X. Huang, J. Yang, G. Qiu, L. Qu, S. Zhao, Z. Luo, X. Wang, Y. Jiu, H. Mao, X. Ding, J. Tan, Y. Hu, L. Pan, L. Chen and H. Li, *bioRxiv*, 2022, DOI: **10.1101/2022.12.01.518675**.

179 M. S'Ari, J. Cattle, N. Hondow, H. Blade, S. Cosgrove, R. M. Brydson and A. P. Brown, in *Journal of Physics: Conference Series*, Institute of Physics Publishing, UK, 2015, vol. 644, p. 012038.

180 M. Karuppasamy, F. Karimi Nejadasl, M. Vulovic, A. J. Koster and R. B. G. Ravelli, *J. Synchrotron Radiat.*, 2011, **18**, 398–412.

181 J. Cheng and X. Zhang, *Biophys. Rep.*, 2021, **7**, 152–158.

182 J. Lv, H. Zhang, D. Zhang, L. Liu and Y. Han, *Acc. Mater. Res.*, 2022, **3**, 552–564.

183 A. S. Frangakis, *J. Struct. Biol.*, 2021, **213**, 107804.

184 B. Salmon and A. Krull, in *Lecture Notes in Computer Science*, Springer, Cham, Switzerland, 2023, p. 13804.

185 A. Krull, T.-O. Buchholz and F. Jug, in *2019 IEEE/CVF Conference on Computer Vision and Pattern Recognition*, Institute of Electrical and Electronics Engineers, USA, 2019, pp. 2124–2132.

186 T. Bepler, K. Kelley, A. J. Noble and B. Berger, *Nat. Commun.*, 2020, **11**, 5208.

187 A. Cheng and Y. Yu, *Curr. Opin. Struct. Biol.*, 2024, **86**, 102795.

188 A. Shah, J. A. Schiller, I. Ramos, J. Serrano, D. K. Adams, S. Tawfick and E. Ertekin, *Mater. Today Commun.*, 2023, **35**, 106127.

189 L. Yao, H. An, S. Zhou, A. Kim, E. Luijten and Q. Chen, *Nanoscale*, 2022, **14**, 16479–16489.